Fritz Schuermeyer et. al. "Photometry and Radiometry."

Copyright 2000 CRC Press LLC. <http://www.engnetbase.com>.

Fritz Schuermeyer
Wright Patterson Air Force Base

Thad Pickenpaugh
Wright Patterson Air Force Base

Michael R. Squillante
Radiation Monitoring Devices, Inc.

Kanai S. Shah
Radiation Monitoring Devices, Inc.

J.A. Nousek
Pennsylvania State University

M.W. Bautz
Pennsylvania State University

B.E. Burke
Pennsylvania State University

J.A. Gregory
Pennsylvania State University

R.E. Griffiths
Pennsylvania State University

R.L. Kraft
Pennsylvania State University

H.L. Kwok
Pennsylvania State University

D.H. Lumb
Pennsylvania State University

Photometry and Radiometry

56.1 Photoconductive Sensors
Introduction • Detector Performance Parameters • Preparation and Performance of Photoconductive Detectors • Instrumentation • References

56.2 Photojunction Sensors
Introduction • Theory • I–V Characteristics of Photodiodes • Position Sensitive Photodiode Arrays • Phototransistors • Novel Silicon Photojunction Detector Structures • Novel Materials for Photodiodes and Bandgap Engineering • Defining Terms • References

56.3 Charge-Coupled Devices
Introduction • CCD Structure and Charge Transport • Applications of CCDs to Light Sensing • References

56.1 Photoconductive Sensors

Fritz Schuermeyer and Thad Pickenpaugh

Introduction

Photoconduction has been observed, studied, and applied for more than 100 years. In the year 1873, W. Smith [1] noticed that the resistance of a selenium resistor depended on illumination by light. Since that time, photoconduction has been an important tool used to evaluate materials properties, to study semiconductor device characteristics, and to convert optical into electric signals. The Radio Corporation of America (RCA) was a leader in the study and development of photoconductivity and of photoconductive devices. Richard H. Bube of RCA Laboratories wrote the classic book ***Photoconductivity in Solids*** [2] in 1960. Today, photoconducting devices are used to generate very fast electric pulses using laser pulses with subpicosecond rise and fall times [3]. For optoelectronic communications, photoconducting devices, allow operation in the gigabit per second range.

Photoconductive devices normally have two terminals. Illumination of a photoconductive device changes its resistance. Conventional techniques are used to measure the resistance of the photoconductor. Frequently, small changes in conductivity need to be observed in the study of material or device characteristics. Also, in the measurement of light intensities of faint objects, one encounters small photoconductive signals.

© 1999 by CRC Press LLC

Only solid photoconductors, such as Si, PbS, PbSe, and HgCdTe, will be treated here. Photoconduction has been observed in amorphous, polycrystalline, and single-crystalline materials. During the last decade, major improvements in materials growth have occurred which directly translate in better device performance such as sensitivity and stability. Growth techniques such as molecular beam epitaxy (MBE) and metal organic chemical vapor deposition (MOCVD) allow the growth of single-crystal layers with an accuracy of the lattice constant. Artificially structured materials can be fabricated with these growth techniques for use in novel photoconducting devices.

Absorption of light in semiconductors can free charge carriers that contribute to the conduction process. Figure 56.1 presents the band diagram for a direct bandgap semiconductor where the excitation processes are indicated. Excitation process (a) is a band-to-band transition. The photon energy for this excitation has to exceed the bandgap of the semiconductor. The absorption constant is larger for this process than for any of the other processes shown in this figure. Typical semiconductors used for electronic applications have bandgaps in excess of 1 eV, corresponding to light in the near-infrared region. Special semiconductors have been developed with narrower bandgaps to provide absorption in the mid- and long-wavelength infrared regions. Indium antimonide (InSb) and mercury-cadmium-telluride (HgCdTe) semiconductors provide photosensitivity in the 4- and 10-μm wavelength range, respectively. The photogenerated carriers increase the electron and hole densities in the conduction and valence bands, respectively, which leads to an increase in conductivity [4]. For the simplified case with one type of carrier dominating, the conductivity σ is given by:

$$\sigma = ne\mu \tag{56.1}$$

where n is the density of free carriers, e their charge and μ their mobility. Absorption of light results in a change in free carrier density and a corresponding change in conductivity $\Delta\sigma$:

$$\Delta\sigma = \Delta ne\mu + \Delta\mu en \tag{56.2}$$

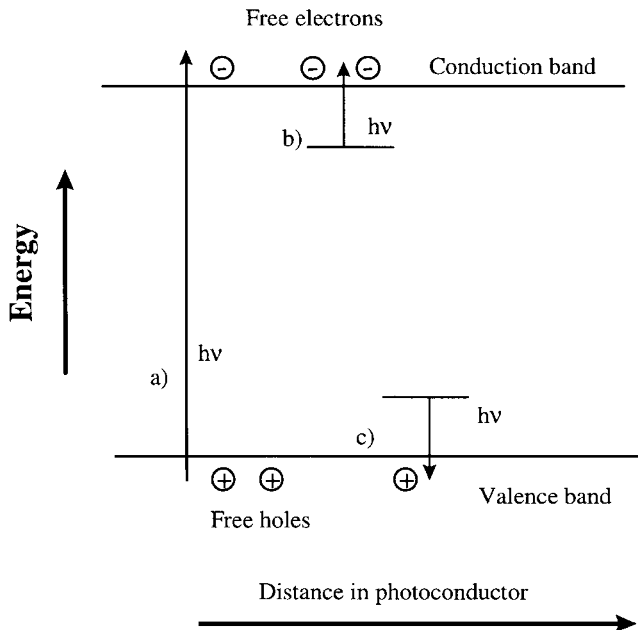

FIGURE 56.1 Example of electronic transitions in a photoconductor: (a) band-to-band excitation, (b) excitation from a trap or a donor, and (c) transition from a trap or an acceptor to the valance band; hν is the energy of the absorbed photon.

© 1999 by CRC Press LLC

$\Delta\sigma$ is the definition for photoconductivity. In Eq. 56.2, one assumes that due to the photon absorption the density of carriers changes. Also, the mobility of the carriers changes due to the modified free carrier density. The latter effect is very small except for special band transitions, as with InSb at very low temperatures.

Figure 56.1 indicates that other excitation processes exist. For example, bound electrons can be excited into the conduction band. This process can lead to persistent photoconductivity. In this example, the trapped holes have a long lifetime while the electrons move freely due to the applied electric field. Charge neutrality requires that the electrons collected at the anode be replenished by electrons supplied by the cathode. This effect leads to an amplification of the photogenerated charge (i.e., more than one electron is collected at the anode of the photoconducting device per absorbed photon). Often, the storage times are long, in the millisecond range. Hence, photoconductive devices with large amplification have a slow signal response.

Small bandgap semiconductors, such as HgCdTe and InSb, are difficult to manufacture. Thus, artificially structured layers of commonly used materials are being developed to replace these. Spatial modulation of doping has been proposed by Esaki and Tsu [5] to achieve a lattice containing a superlattice of ***n***-doped, undoped, ***p***-doped, and undoped layers ***(n-I-p-I)***. Due to the energy configuration of this structure, the effective bandgap is less than that of the undoped material. The effective bandgap depends on the thickness of the layers and their doping concentrations. The quantum-well infrared photodetector (QWIP) [6] is another approach to obtain photoconduction in the far-infrared wavelength range. In this structure, energy wells exist in the conduction band of the material heterostructure due to the energy band discontinuities. Subbands form in the superlattice and electrons in these wells are confined due to

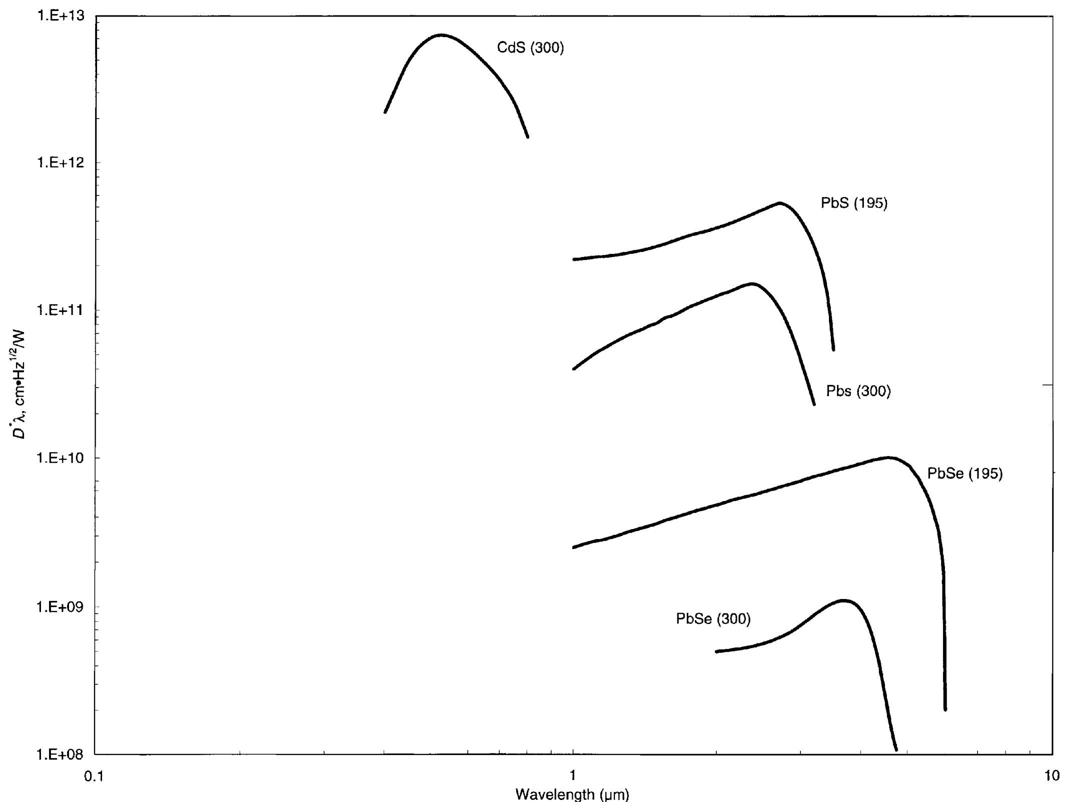

FIGURE 56.2a Absolute spectral response of photoconductive detectors with the operating temperatures in K in parentheses: CdS visible and Pb salt IR detectors. ***(continues)***

© 1999 by CRC Press LLC

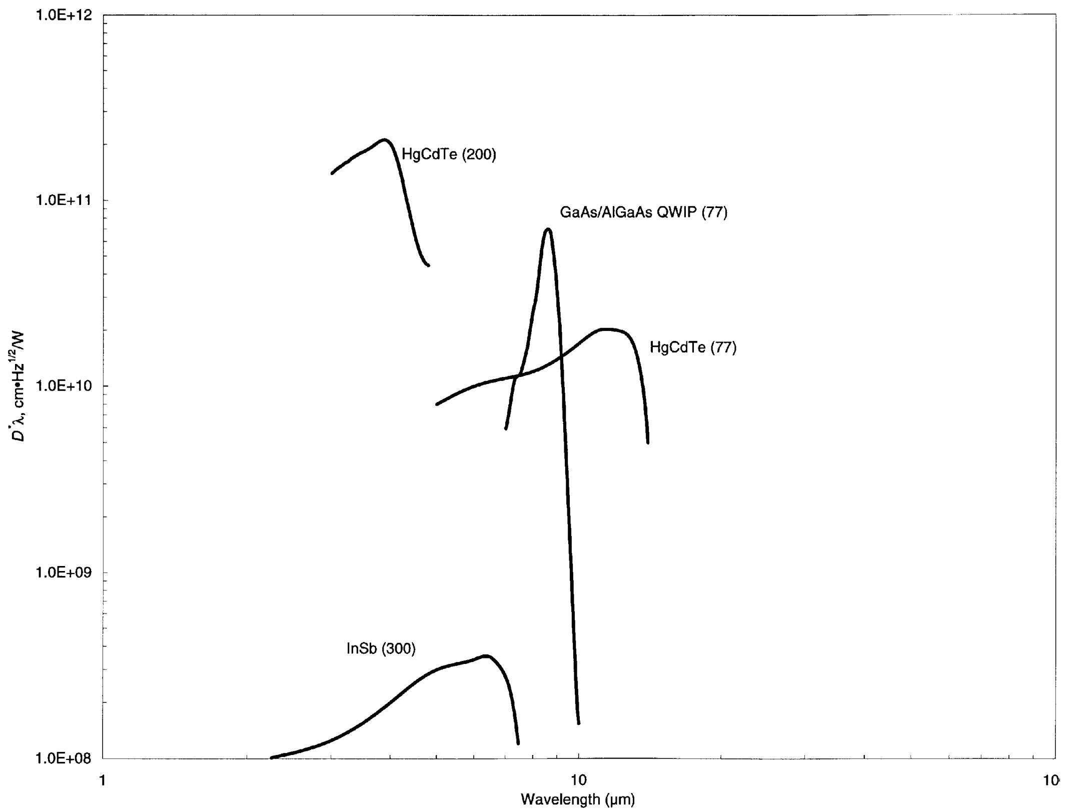

FIGURE 56.2b Absolute spectral response of photoconductive detectors with the operating temperatures in K in parentheses: III–V and II–VI intrinsic photoconductors plus a III–V QWIP detector. ***(continues)***

the heterobarriers. Infrared photons can excite electrons from their confined states to the continuum, which leads to an increase in conductivity.

While it is possible to use noncontact methods to measure the conductivity in a material, electric contacts are commonly placed onto the structure during the device fabrication process. Typically, ohmic contacts are formed to fabricate metal-semiconductor-metal (MSM) structures (Figure 56.2). These contacts control the Fermi level in the material structure and provide carriers to retain charge neutrality.

Detector Performance Parameters

Responsivity

Variations in photon flux density incident on a photoconductor interact with the material to change the conductivity. These changes produce a signal voltage that is proportional to the input photon flux density. The detector area A collects flux contributing to the signal. J_s is the integrated power density over a spectral interval. Responsivity (R_v) is the ratio of the rms signal voltage (or current) to the rms signal power and is expressed in units of volts per watt. It is expressed as amps per watt for current responsivity.

$$Rv = V_s/AJ_s \tag{56.3}$$

V_s is normally linear with photon flux for low levels, but can saturate under high flux conditions. One should ensure operation in the linear range for radiometric and photometric instrumentation.

Noise

The performance of a visible or IR instrument is ultimately limited when the signal-to-noise ratio equals one (SNR = 1). The noise from the instrument's signal processing should be less than the noise from the

© 1999 by CRC Press LLC

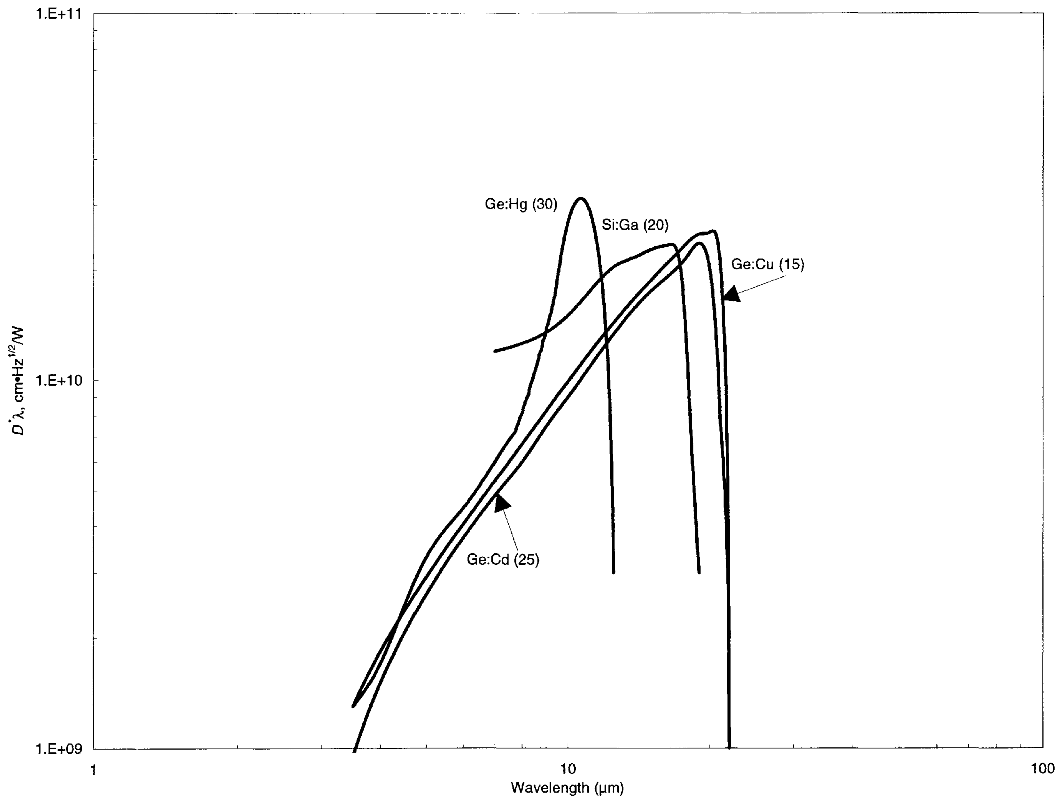

FIGURE 56.2c Absolute spectral response of photoconductive detectors with the operating temperatures in K in parentheses: long-wavelength extrinsic Ge and Si photoconductors.

detector in the ideal case. This means reducing this noise within the restrictions of signal processing design limitations. These may include cost, size, and input power. The detector noise should be minimized.

Johnson noise is the limiting noise in all conductors [7]. It is frequency independent, and independent of the current going through the device. Johnson noise is defined in Equation 56.4, where $\boldsymbol{k}$ is the Boltzmann constant (1.38×10^{-23} J/K), $\boldsymbol{T}$ is the detector temperature (K), $\boldsymbol{R}$ is the resistance (Ω), and Δf is the amplifier bandwidth (Hz).

$$V_{\mathrm{J}} = \sqrt{(4kTR\Delta f)} \tag{56.4}$$

Another type of noise known as $1/f$ noise (V_f) is present in all semiconductor detectors that carry current. The spectrum of this noise varies as $1/f^n$, with $\boldsymbol{n}$ approximately 0.5 [8].

Noise due to fluctuation in generation and recombination of charge carriers [9] varies linearly with current. This noise may be caused by the random arrival of photons from the background (photon noise), fluctuation in the density of charge carriers caused by lattice vibration (*g-r* noise), by interaction with traps, or between bands.

Excess noise from the amplifier or signal processing (V_{amp}) can also limit photoconductive detector performance.

These uncorrelated noises add in quadrature, giving the total noise (V_{N}):

$$V_{\mathrm{N}}^2 = V_{\mathrm{J}}^2 + V_{\mathrm{g-r}}^2 + V_{\mathrm{amp}}^2 \tag{56.5}$$

© 1999 by CRC Press LLC

The total noise may be given in units of $\mathrm{V}\sqrt{\mathrm{Hz}}$. It may also be integrated over some frequency range to provide volts rms. Photoconductive detectors often have a ***g-r*** noise independent of frequency from dc to 100 kHz.

Detector Sensitivity

Minimum detectable signal power, that is, Noise Equivalent Power (NEP) is a convenient means to express detector sensitivity. NEP is expressed in units of watts or $\mathrm{W}\sqrt{\mathrm{Hz}}$.

$$\mathrm{NEP} = V_{\mathrm{N}} / R_{\mathrm{V}} \tag{56.6}$$

The reciprocal of NEP, the detectivity ***D*** is frequently used. In attempting to make possible comparison among detectors, detectivity can be normalized to an electronic bandwidth of 1 Hz and a detector area of 1 cm^2. This yields the highly used parameter specific detectivity or D^* (pronounced "dee-star") [10]:

$$D^* = (R_{\mathrm{V}} / V_{\mathrm{N}})\sqrt{(A \Delta f)} \tag{56.7}$$

The units of D* are cm · $\mathrm{Hz}^{1/2}$/W, sometime simplified to "Jones".

This normalization is based on evidence that noise varies as the square root of the electronic bandwidth and ***D*** varies inversely as the square root of the detector area. This relationship may not hold closely over a wide range of device sizes and bandwidths. Comparison of device performance is most meaningful among devices having similar sizes and measured under similar conditions, including operating temperature, chopping frequency/scanning rate, and detector field of view.

Preparation and Performance of Photoconductive Detectors

Cadmium Sulfide

CdS is normally prepared by vapor deposition or sintering a layer of high-purity CdS powder on a ceramic substrate [11]. It has the largest change in resistance with illumination of any photoconductor. The peak response of this intrinsic detector is at 0.5 µm. Its spectral response is similar to that of the human eye and operates without cooling.

Lead Sulfide

PbS was among the earliest IR detector material investigated. Cashman was one of the earliest researchers in the U.S. [12]. This intrinsic detector material is prepared by deposition of polycrystalline thin films by vacuum sublimation or chemical deposition from a solution. The spectral response extends to approximately 3 µm. PbS operates over the temperature range from 77 K to room temperature. The frequency response slows considerably at the lowest temperatures. The spectral response extends to somewhat longer wavelengths with cooling.

Lead Selenide

PbSe is an intrinsic detector that operates over the temperature range from 77 K to room temperature. Its spectral response extends to longer wavelengths with cooling. Preparation of PbSe is by sublimation or chemical deposition. Noise in PbSe detectors follows a $1/f$ spectrum.

Indium Antimonide

InSb is prepared by melting together stoichiometric quantities of indium and antimony. It operates over the range from 77 K to room temperature. The higher performance and ease of operation with signal processing electronics lead photovoltaic InSb detectors to be much more widely used than photoconductive.

Mercury Cadmium Telluride

HgCdTe is a versatile intrinsic material for IR detectors. CdTe and HgTe are combined to form the alloy semiconductor $Hg_{1-x}Cd_xTe$. For the alloy with $x \approx 0.2$, the bandgap is approximately 0.1 eV, providing a

© 1999 by CRC Press LLC

long wavelength cutoff of 12.4 μm. HgCdTe was initially grown into bulk crystals by solid-state crystallization (also called quench and anneal). Currently, thin film growth techniques of liquid phase epitaxy (LPE), MOCVD, and MBE are preferred to obtain larger, more uniform wafers. By appropriately choosing the alloy composition, photoconductive HgCdTe detectors are possible over the 2- to 20-μm range. CdZnTe wafers permit lattice-matched surfaces for HgCdTe thin film growth. Operating temperatures can range from 77K to room temperature, with the lower temperatures necessary for the longer wavelength devices.

Extrinsic Germanium and Silicon

The photoresponse of an extrinsic detector occurs when a photon interacts with an impurity added to a host semiconductor material. With an intrinsic material, the photoresponse is from the interaction with the basic material.

For the extrinsic detector, incident photons may produce free electron-bound hole pairs, or bound electron-free hole pairs. The extrinsic detector's spectral response is achieved using an impurity (or doping element). Intrinsic detection occurs with a detector having the necessary bandgap width for the desired spectral response.

Extrinsic detectors require lower temperatures than do intrinsic and QWIPs, but have the advantage of longer wavelength response.

Ge and Si are zone refined to achieve high purity by making multiple passes of a narrow molten zone from one end to the other of an ingot of the material. Unwanted impurities can be reduced to levels of 10^{12} to $10^{13}/m^3$ [13]. Growth of single crystals is by the Czochralski approach of bringing an oriented seed crystal in contact with the melt and withdrawing it slowly while it is rotated, or by applying the horizontal zone refining approach, whereby an oriented seed crystal is melted onto the end of a polycrystalline ingot. A molten zone is started at the meeting of the ingot and seed and moved slowly down the ingot, growing it into a single crystal. An inert atmosphere is required to prevent oxidation.

Hg, Cd, Cu, and Zn are impurities for doping Ge detectors; Ga and As are dopants for Si detectors. See Table 56.1 and Figure 56.3.

TABLE 56.1 Photoconductive Detectors

Material	Cutoff Wavelength (μm)	Temp (K)	Responsivity (V/W)	D* (cm Hz$^{1/2}$/W)
CdS	0.7	300	1×10^6	1×10^{13}
PbS	3	300	$5 \times 10^4 - 1 \times 10^3$	$5 \times 10^{11} - 1 \times 10^{11}$
PbSe	5.8	77–300	$1 \times 10^6 - 1 \times 10^3$	$2 \times 10^{10} - 7 \times 10^8$
InSb	7	300	5	4×10^8
HgCdTe	5	150–220	$1 \times 10^5 - 2 \times 10^4$	
HgCdTe	12	65–100	1×10^5	3×10^{10}
Ge:Hg	13	4–25	8×10^5	2×10^{10}
Ge:Cd	24	20–30	5×10^5	2×10^{10}
Ge:Cu	33	5	5×10^5	3×10^{10}
GaAs/AlGaAs (QWIP)	9	77	780 mA/W	7×10^{10}

From References 14 and 15.

Gallium Arsenide/Aluminum Gallium Arsenide QWIP

QWIP technology uses a quantum-well structure to provide intraband (intersubband) transitions to achieve an effective long-wavelength response in a wide bandgap material. Quantum wells are used to provide states within the conduction or valence bands. Since hυ of the desired spectral region is less than the bandgap of the host material, the quantum wells must be doped. Quantum-well structures are

© 1999 by CRC Press LLC

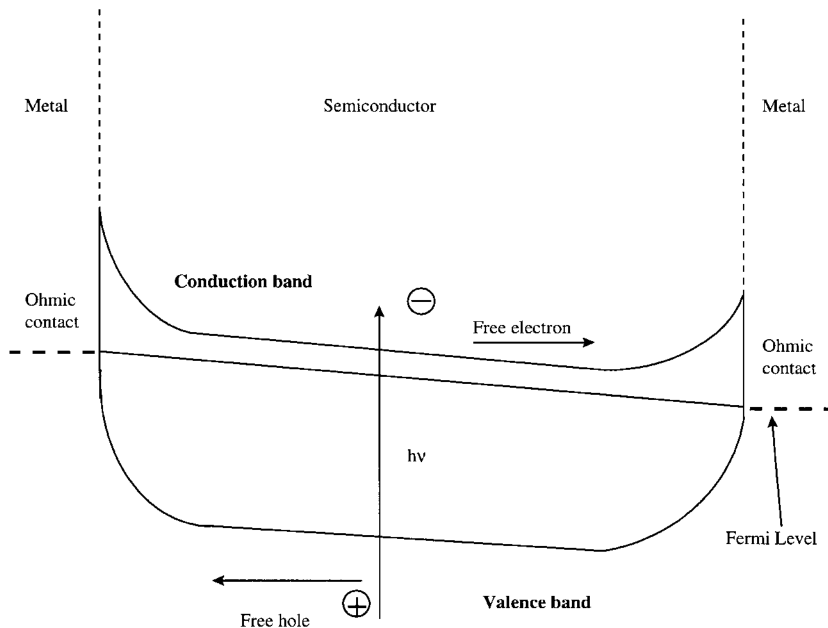

FIGURE 56.3 Energy diagram for a metal-semiconductor-metal (MSM) detector.

designed to permit photoexcited carriers to depart the structure, and be accumulated as signal (photocurrent). The QWIP detector is generally comparable to extrinsic photoconductive detectors [16], in that both have lower than desirable quantum efficiency. GaAs/AlGaAs QWIPs have the advantage of higher operating temperatures than extrinsic detectors.

Instrumentation

The Stanford Research Systems SR570 low-noise current preamplifier can be used to amplify the current flowing through a photoconductive device. This preamplifier can be programmed to apply a voltage to the terminals of the photoconducting device. Its output voltage is proportional to the device current. Frequently, the IR radiation or visible light is chopped and the ac component of the device current is detected using lock-in-amplifier techniques. This approach allows the study of very small changes in device conduction. The Stanford Research Systems SR570 and the EG&G Instruments Model 651 are examples of a lock-in amplifier and a mechanical radiation/light chopper, respectively.

References

1. W. Smith, *Nature*, 303 (1873).
2. R.H. Bube, *Photoconductivity of Solids*, New York: John Wiley & Sons, 1960.
3. J.A. Valdmanis, G.A. Mourou, and C.W. Gabel, Pico-second electro-optic sampling system, *Appl. Phys. Lett.*, **41**, 211–212, 1982.
4. R.H. Bube, Photoconductors, in *Photoelectronic Materials and Devices*, S. Larach, Editor, Princeton, NJ, D. Van Nostrand Company, 100–139, 1965.
5. L. Esaki and R. Tsu, Superlattice and negative differential conductivity in semiconductors, *IBM J. Res. Dev.* **14**, 61, 1971.
6. B.F. Levine, Quantum-well Infrared Photodetectors, *J. Appl. Phys.* **74**, R1-R81, 1993.
7. P.W. Kruse, L.D. McGlauchlin, and R.B. McQuistan, *Elements of Infrared Technology*, New York: John Wiley & Sons, 1962.

© 1999 by CRC Press LLC

8. H. Levinstein, Characterization of infrared detectors, in *Semiconductors and Semimetals*, R.K. Willardson and A.C. Beer (Eds.), New York: Academic Press, **5,** 5,1970.
9. K.M. Van Vliet, Noise in semiconductors and photoconductors, *Proc. I.R.E.*, **46**, 1004, 1958.
10. R.C. Jones, Phenomenological description of the response and detecting ability of radiation detectors, *Proc. I.R.E.*, **47**, 1495, 1959.
11. p. 417–418 of Reference 7.
12. R.J. Cashman, Film-type infrared photoconductors, *Proc. I.R.E.,* **47**, 1471, 1959.
13. S.R. Borrello and M.V. Wadsworth, Photodetectors in *Encyclopedia of Chemical Technology*, R.E. Kirk and D.E. Othmer (Eds.), New York: John Wiley & Sons, **18**, 897–898, 1996.
14. p. 862-863 of Reference 13.
15. W.L. Wolfe and G.J. Zissis (Eds.), *The Infrared Handbook, revised ed.,* Ann Arbor, MI: Environmental Research Institute of Michigan, 1985.
16. p. R3 of Reference 6.
17. T.R. Schimert, D.L. Barnes, A.J. Brouns, F.C. Case, P. Mitra, and L.T. Clairborne, Enhanced quantum well infrared photodetector with novel multiple quantum well grating structure, *Appl. Phys. Letts.,* **68** (20), 2846-2848, 1996.

56.2 Photojunction Sensors

Michael R. Squillante and Kanai S. Shah

Introduction

Photojunction sensors (photodiodes and phototransistors) are semiconductor devices that convert the electrons generated by the photoelectric effect into a detectable electronic signal. The ***photoelectric effect*** is a phenomenon in which photons lose energy to electrons in a material. In the case of a semiconductor, when the energy of an interacting photon ($h\nu$) exceeds the energy of the semiconductor bandgap (E_g), the energy absorbed can promote an electron from the valence band to the conduction band of the material. This causes the formation of an electron-hole pair. In the presence of an electric field, these charges drift toward electrodes on the surface and produce the signal.

The junction in the photojunction device creates a diode that provides a small built-in electric field to propel the charges to the electrodes (photovoltaic mode of operation). In the photovoltaic mode, either the photocurrent or the photovoltage can be measured. This mode of operation provides very high sensitivity because there is no net reverse leakage current, but relatively poor frequency response occurs because of high capacitance and low electric field.

Photodiode devices are most often operated with a bias voltage applied opposing the junction (***reversed bias***) to provide the electric field. The presence of the junction in a diode allows for the application of a relatively large bias to be applied while maintaining a relatively low reverse leakage current and thus relatively low noise. The result of an applied bias on a junction is the increase of the "depletion region," which is the sensitive volume of the detector. Any charges that are generated within this volume are swept toward the electrodes by the field, adding to the reverse leakage current. The ***total reverse*** current is the sum of the ***dark current,*** which occurs due to thermal generation of charges in the depletion region, and the ***photocurrent,*** which is produced due to optical illumination. Thus, the lower the dark current, the higher the sensitivity of the detector to optical illumination.

In an ideal diode, all of the light incident on the photodiode surface is converted to electron-hole pairs and all of the charges drift to the electrodes and are collected. In a real device, there are reflection losses at the surface, additional light is lost in the electrode and/or front layers of the device, and not all of the charges are collected at the electrodes.

There are several fundamental types of junction photodiodes [1], as shown in Figure 56.4. A ***Schottky barrier*** diode is a device in which the junction is formed at the surface of the semiconductor by the

© 1999 by CRC Press LLC

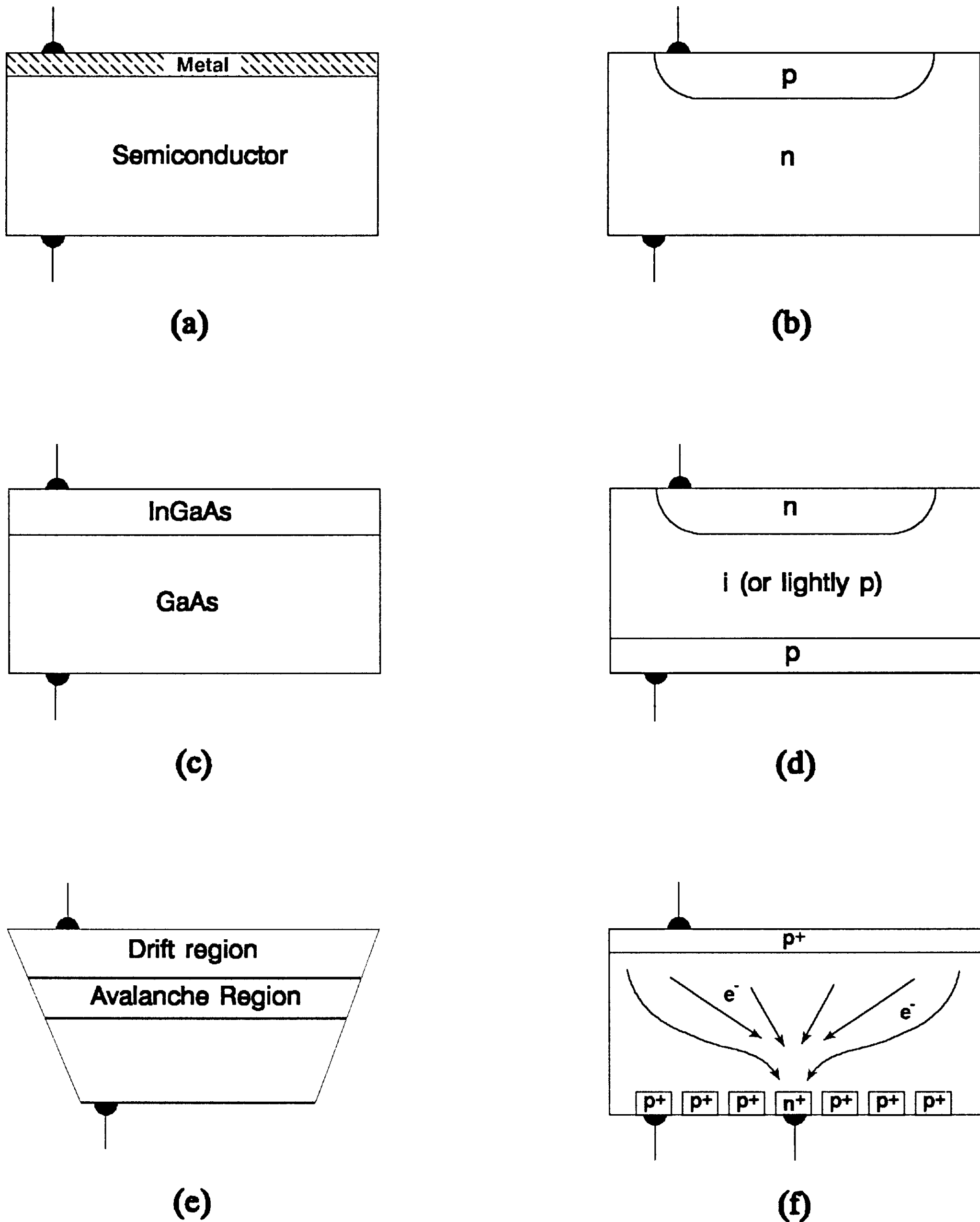

FIGURE 56.4 Schematic of photodiode device structures: (a) Schottky junction, (b) homojunction, (c) heterojunction, (d) *p-i-n*, (e) APD, (f) drift diode.

application of a metal electrode that has a work function that is different from the work function of the semiconductor; a ***heterojunction diode*** is a device in which two different semiconductor materials with differing work functions are joined; a ***homojunction diode*** is a device in which the junction is created at an interface in a single material and the difference in work function is created by doping the material *n*-type and *p*-type. Most photodiodes are homojunction devices made using silicon. Other, more complex types of photojunction devices, which are discussed below, include ***p-i-n photodiodes, avalanche photodiodes*** (APD), ***drift photodiodes,*** and ***phototransistors.***

© 1999 by CRC Press LLC

Photodiodes are typically characterized by several properties, including bandwidth, spectral response, operating bias, operating temperature, dark current, junction capacitance, noise equivalent power, and peak wavelength. Other specifications usually provided by manufacturers include size, packaging details, operating temperature range, capacitance, and price.

Photodiodes are used in numerous applications, including CD-ROM systems, television remote control systems, fax machines, copiers, optical scanners, fiber optic telecommunication repeaters, surveillance systems such as motion detectors, certain smoke detectors, light meters, and a wide variety of scientific instrumentation including spectrophotometers, scintillation detectors, optical trackers, laser range finders, LIDAR, LADAR, analytical instrumentation, optical thermometers, nephelometers, densitometers, radiometers laser detectors, shaft encoders, and proximity sensors. Photodiode arrays are available for use as position-sensitive detectors that can either be used for imaging (such as in laser scanners, night vision equipment, spectrophotometers, and edge detection) or alignment systems. Medical imaging applications such as x-ray CT scanners also use large arrays of photodiodes.

A variety of materials are used in the fabrication of photodiodes, but most are fabricated using silicon. Other materials used include CdS, Se, GaAs, InGaAs, HgCdTe, and PbS. In addition, materials with unique properties can be used to solve very specific and unusual problems, including Ge, GaP, HgMnTe, InP, HgI2, and InI.

Photodiodes are an alternative to photomultiplier tubes in many applications. There are a variety of advantages to be gained—including higher quantum efficiency, tailored spectral response, increased ruggedness, reduced power requirements, reduced weight, compact size, elimination of warm-up period, reduced sensitivity to temperature and voltage fluctuations, and insensitivity to magnetic fields. In general, photodiodes are noisier and require more sophisticated readout electronics than photomultiplier tubes, especially at room temperature. Upon cooling, the noise in photodiodes can be reduced significantly due to reduction in dark current.

Figure 56.5(a) shows a simple circuit for operating a photodiode in the photovoltaic mode. In this mode, photocurrent is usually measured because the photocurrent is nearly proportional to the input signal. The output of the photodiodes is typically connected to the input of an op-amp current-to-voltage converter. Figure 56.5(b) shows a simple circuit for operating a photodiode under reverse bias.

Table 56.2 shows a few examples of available photodiodes. These are only a small fraction of the commercially available photodiodes and photodiode manufacturers. Lists of photodiode manufacturers are available [2,3].

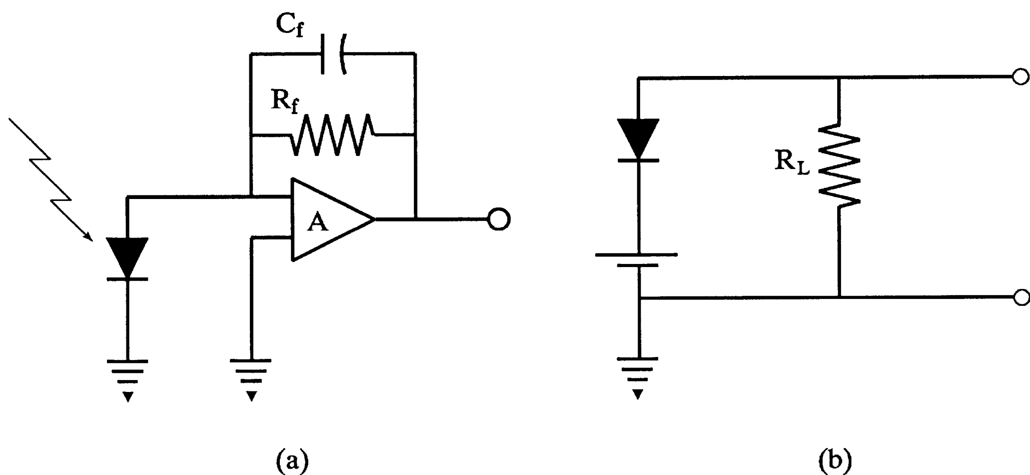

FIGURE 56.5 Typical circuits for operation of a photodiode: (a) circuit for photodiode operation in photovoltaic mode, (b) circuit for photodiode operating under reverse bias.

© 1999 by CRC Press LLC

TABLE 56.2 Examples of the Variety of Commercially Available Photodiodes

Commercial source	Type	Region	Example device	Comments
Hamamatsu	Si	Visible	S2386-44K	13 mm^2, \$13
UDT	Si-*p-i-n*, UV enhanced	To 200 nm	UV50	50 m^2, \$44
UDT	Si-*p-i-n*	Visible	PIH-HS040	0.8 mm^2, fast, \$18
Hamamatsu	Si APD	Visible	S2385	20 mm^2, \$560
RMD	Si APD	Visible	SH8S	169 mm^2, \$2850
UDT	InGaAs	Near IR	InGaAs-300	0.1 mm^2, \$69
Lasertron	InGaAs *p-i-n*	1.3–1.55 μm	QDEP	\$200–250
Hamamatsu	GaP	Near UV	G1961	1 mm^2, \$42
Hamamatsu	GaAsP	Near UV and visible	G1125-02	1 mm^2
Brimrose	HgMnTe	2 to 12 μm	MMT-212-3-1	0.8 mm^2, \$2240
Komar	HgCdTe	2 to 12 μm	KV104-1-a	1 mm^2, \$3550
Komar	HgCdTe	to 18 μm	KMPC18-1-b1	1 mm^2, \$2000
Komar	InSb	5.1 μm	KISD-1-a	1 mm^2, \$2100

Note: Brimrose Corp. of America, Baltimore, MD; Hamamatsu, Corp. Bridgewater, NJ; Kolmar Technologies, Conyers, GA; Lasertron Corp, Burlington, MA; Loral Lexington, MA; RMD = Radiation Monitoring Devices, Inc., Watertown, MA; UDT = UDT Sensors, Inc., Hawthorne, CA.

Theory

Equivalent Circuit

A simplified version of the equivalent circuit for a photodiode is shown in Figure 56.6, where C_j = junction capacitance, I_d = dark current (current present with no incident photons), I_j = reverse saturation current, I_o = output current, I_p = photocurrent current, R_j = junction shunt resistance (or parallel resistance), R_s = series resistance, V_j = junction voltage, V_o = output voltage.

The dark current from this structure is ideally given by:

$$I_d = I_j\{\exp((qV_j/kT) - 1)\} \tag{56.8}$$

where k = Boltzmann's constant, q = electronic charge, T = absolute temperature.

Total current under illumination is given by:

$$I_o = I_d + I_p \tag{56.9}$$

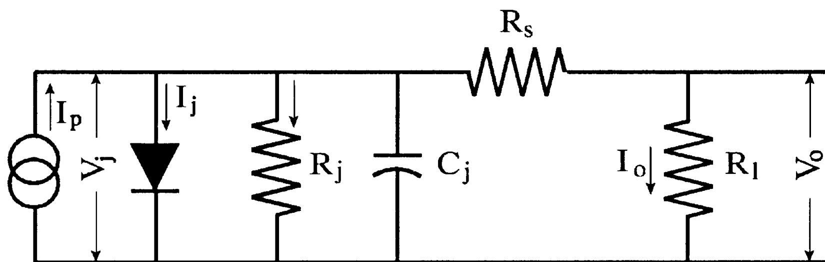

FIGURE 56.6 Equivalent circuit for a photodiode.

© 1999 by CRC Press LLC

For a more rigorous treatment refer to Reference 1, pp. 752–754.

Quantum Efficiency

The ***quantum efficiency*** of a photodiode is the ratio of the charge pairs generated to the incident photons:

$$\eta = (I_p/q)/(P_i/h\upsilon) \tag{56.10}$$

Where P_i = optical power incident on the photodiode, $h\upsilon$ = energy of the photons.

The responsivity, $\mathcal{R}$ is the ratio of the photocurrent to the incident optical power in amps/watt:

$$\mathcal{R} = I_p/P_i = \eta q/h\upsilon \tag{56.11}$$

The photocurrent is given by rearranging Equation 56.9:

$$I_p = q\eta P_i/h\upsilon \tag{56.12}$$

Noise

There are two main sources of noise when using a photodiode: shot noise in the diode and thermal noise. The ***shot noise*** is related to the dark current by the formula:

$$I_s = (2qI_dB)^{1/2} \tag{56.13}$$

where B = bandwidth.

Assuming the diode shunt resistance and the input resistance of the measuring circuit to be used to measure the output of the photodiode are high relative to the load resistance, the thermal noise is given by:

$$I_t = (4kTB/R_L)^{1/2} \tag{56.14}$$

where R_L = load resistance. The total noise current, I_n, is the sum of these currents in quadrature.

I–V Characteristics of Photodiodes

With no illumination, photodiodes have I–V curves equivalent standard diodes given by Equation 56.8. Illumination by light causes the current to increase. Figure 56.7 shows a family of I–V curves for a photodiode under illuminations with equally increasing increments of incident light intensity. As the illumination on the device increases, the curve shifts downward by the amount of current generated by the incident light. The lower right-hand quadrant represents the photovoltaic mode of operation. When a photovoltaic device is operated in "current mode" with low or no load resistance (as with an operational amplifier, as in Figure 56.5(a) above), the output is linear with incident light intensity. When operated in "voltage mode" with a high load resistance, there is an exponential relationship between the output and the incident illumination. The lower left-hand quadrant shows the reversed bias mode of operation. Again, in this mode the output is nearly linear with the incident intensity.

Output Current Under Reverse Bias

In a reverse bias ***p-n*** junction under bias, the depletion width (W) increases as a function of applied bias (V_b) until the device is fully depleted. The dark leakage current (I_d) under reverse bias conditions can arise from the generation-recombination effects (I_G) and from diffusion (I_D) as well as surface effects. In most cases, the diffusion current is significantly smaller than the generation-recombination component. Thus, it is possible to assume that $I_d \approx I_G$.

The analytical expression for I_G is as follows:

© 1999 by CRC Press LLC

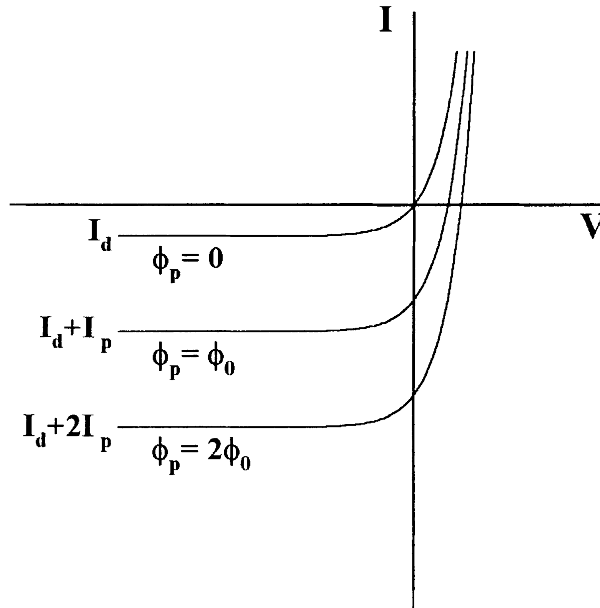

FIGURE 56.7 I–V characteristics of photodiode under illumination.

$$I_G = AWqn_i/2\tau \tag{56.15}$$

where: A = device area, n_i = intrinsic carrier concentration, τ = minority carrier lifetime.

The total diode current under illumination (I_o) is the sum of the dark leakage current (I_d) and the photocurrent (I_P):

$$I_o = I_d + I_P \tag{56.16}$$

Position Sensitive Photodiode Arrays

Many manufacturers offer photodiodes fabricated in a ***quadrant*** geometry. Four photodiodes are fabricated in a square, 2 × 2 geometry. When coupled to a lens or a pinhole, they can be operated as position sensitive detectors. In operation, the outputs of the four photodiodes are monitored and the position of the light source can be determined by the projection of the light spot on the detector surface. More recently, manufacturers are offering linear and area arrays of photodiodes that can be used as imaging devices.

Phototransistors

Phototransistors are photojunction devices similar to transistors except that the signal amplified is the charge pairs generated by the optical input. Like transistors, phototransistors can have high gain. Phototransistors can be made on silicon using ***p***- and ***n***-type junctions or can be heterostructures. Figure 56.8 shows a sketch of the structure of a simple bipolar phototransistor, which is essentially the same as that of a simple bipolar transistor. The main difference is the larger base-collector junction, which is the light-sensitive region. This results in a larger junction capacitance and, although the devices have gain, the capacitance gives phototransistors lower frequency response than photodiodes.

© 1999 by CRC Press LLC

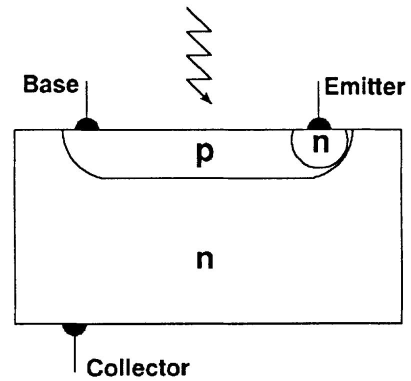

FIGURE 56.8 Schematic representations of a simple bipolar phototransistor. Note that the phototransistor has a large *p-n* junction region that is the photosensitive portion of the device.

Using thin film transistor (TFT) technology developed for flat panel displays, large arrays of phototransistors can be fabricated on amorphous silicon to form imaging devices that can be used in place of other imaging technologies such as vidicon tubes or even film. Examples of this are the very large area detectors (hundreds of square centimeters) being investigated for use in medical radiography by combining the TFT arrays with radiographic phosphor screens [4] or coupled to semiconductor films [5].

Novel Silicon Photojunction Detector Structures

Silicon *p-i-n* Detectors

Silicon *p-i-n* diodes are an extension of the standard *p-n* junction diodes, but are more attractive for low-noise applications due to reduced capacitance in these devices [1]. The reduction in capacitance is achieved by incorporating an intrinsic region between the *p* and *n* regions. This increases the depletion width of the detector and thereby lowers its capacitance. Silicon *p-i-n* detectors can be designed to have higher frequency response than *p-n* junctions and therefore are more popular.

In operation, *p-i-n* detectors are similar to *p-n* junction detectors, but the surface region (either *p* or *n*) is made thin so that the optical photons penetrate this entrance layer and are stopped in the intrinsic (*i*-region) where electron-hole pairs are produced, as shown in Figure 56.4. These electron-hole pairs are swept toward the appropriate electrodes due to applied electric field. For fabrication, *p-i-n* detectors require high resistivity material and typical photodiodes have thickness ranging from 100 to 500 μm. Important applications of *p-i-n* detectors include optical sensing of scintillated light in CT scanners, general scintillation spectroscopy, charged particle spectroscopy, and high-speed sensing applications.

Silicon Drift Detectors

Silicon drift photodiodes are an extension of the *p-i-n* geometry and been extensively studied in recent years to provide very low capacitance (<1 pF for 1 cm^2 detector with 300 μm thickness) [7]. This is achieved by reducing the area of ohmic electrode (anode in most cases) significantly as compared to the entrance electrode as shown in Fig. 56.4(f). Since the charge sensing electronics is connected to the smaller electrode, the device capacitance is proportional to its size and not to the actual detector area. Thus by exploiting this concept, significantly lower capacitance has been achieved than in comparable *p-i-n* detector.

In drift detectors, it is important to ensure that charges created over the entire active volume will be collected at the anode. In order to achieve this, drift rings are provided around the anode. The outermost ring is biased at highest potential, with the inner rings biased to lower potentials in a successive manner. This arrangement creates a potential minimum at the anode and thereby enables efficient charge collection over the entire detector volume. A variety of device geometries are being explored based on this concept and in some instances these detectors are capable of providing position sensitive detection as well. While these detectors are in the research stage, excellent performance has been demonstrated by prototype detectors. These detectors, when they are commercially available, will have the potential of replacing *p-i-n* diodes in many applications.

© 1999 by CRC Press LLC

Silicon Avalanche Photodiodes

While the conventional silicon diodes, such as ***p-n*** junction diodes, ***p-i-n*** diodes and drift diodes, have no gain, silicon avalanche photodiodes (APDs) have internal gain that enables them to operate with high signal-to-noise ratios and also places less stringent requirements on supporting electronics. In its simplest form, an APD is a ***p-n*** junction operated close to its breakdown voltage in reverse bias. When photons are absorbed in silicon, electron-hole pairs are produced and are accelerated by the high electric field. These electrons gain sufficient velocity to generate additional free carriers by impact ionization, which provides the internal gain. APDs with small areas (few mm diameter) can be manufactured with standard planar processing and have a gain of a few hundred. These detectors are widely used in the telecommunications industry. It is difficult to fabricate high gain detectors with large areas using the planar process; however, special detector designs with beveled edges (see Figure 56.4) have been fabricated to provide high gain (>10,000) in large areas (>1 cm^2) [8]. The APD gain versus bias behavior for such a device is shown in Figure 56.9. Recent advances in surface preparation and dead layer reduction have extended the application of these detectors to the UV region. While they are relatively expensive, these detectors are well suited to a number of commercial applications such as medical imaging, astronomy, charged particle and x-ray detection, scintillation spectroscopy, and optical communications.

Amorphous Silicon Detectors

While impressive results have been obtained with various device structures on crystalline silicon such as drift detectors, APDs, and CCDs, they are limited to active areas of only a few square centimeters. As a result, considerable attention has been devoted to development of hydrogenated amorphous silicon (a-Si:H) [4]. This material is produced by an RF plasma technique in large areas (30 cm × 30 cm) on glass substrates. The films are typically a few micrometers in thickness, although films as thick as 200 μm has been reported. Device structures such as ***p-n*** junctions were developed initially for use in solar cells with lower cost than crystalline silicon devices.

Recently, more complicated devices such as ***p-i-n*** sensors and thin film transistors (TFTs) have been fabricated from a-Si:H and have been configured in an array format as shown in Fig. 56.10. In these arrays (as large as 20 cm × 20 cm), each pixel consists (200 to 500 μm) of a ***p-i-n*** sensor connected to a TFT, and the entire array is read out in matrix fashion. These arrays are well suited for high-resolution document imaging and also for medical x-ray imaging applications with phosphors.

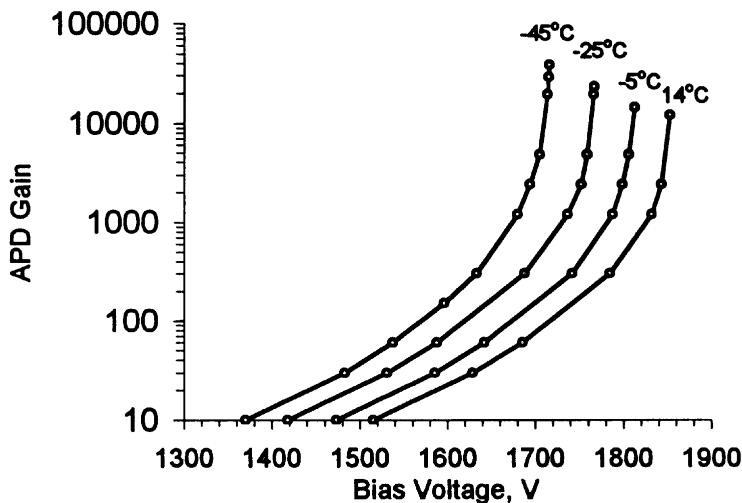

FIGURE 56.9 Gain versus bias relationship for a high-gain APD. Higher gains are achievable at lower voltages as the temperature is decreased.

© 1999 by CRC Press LLC

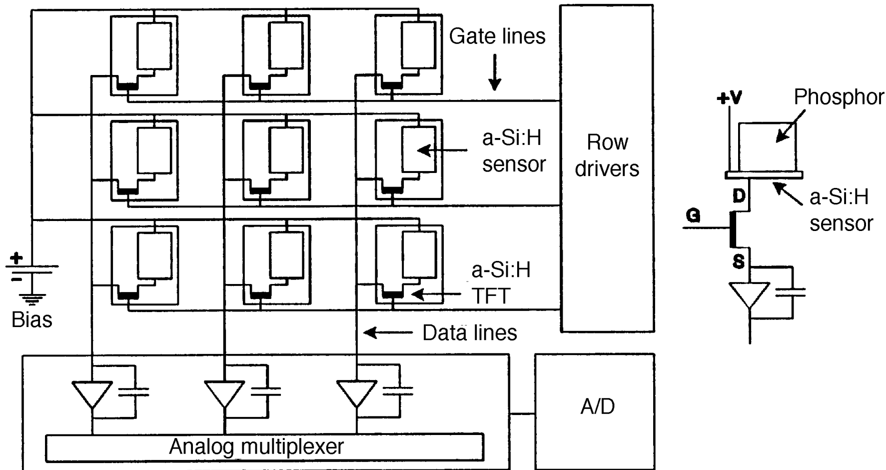

FIGURE 56.10 Schematic representation of a 2-D x-ray imager consisting of a-Si:H ***p-i-n*** diodes connected to a-Si:H TFTs for readout. The ***p-i-n*** diodes are coupled to a phosphor layer to increase sensitivity.

Novel Materials for Photodiodes and Bandgap Engineering

Important requirements for photodiodes include high quantum efficiency (QE), good charge collection efficiency, and low noise. The low noise requirement is satisfied by reducing detector capacitance and its dark current. In order to satisfy the QE requirements over a wide range of wavelengths, new semiconductor materials are being extensively investigated [9]. Since most semiconductors show high optical response near their bandgap, special materials are developed for various applications. Furthermore, since the bandgap represents a cut-off point in the optical response of the material, by selecting an appropriate material, it is possible to obtain response in a desired band [10]. For example, materials such as GaN and SiC are being explored to obtain UV detection with no sensitivity in the visible region. Other materials are being studied to exploit their unique properties such as high quantum efficiency, high-temperature operation, and high-speed response.

GaN

GaN is an attractive material for ***UV photodiode*** fabrication due to its wide bandgap (E_g = 3.4 eV). Due to the difficulty in growing bulk crystals of GaN, much of the work is done with films of GaN prepared by chemical vapor deposition or molecular beam epitaxy [11]. A variety of optical devices (e.g., blue LEDs and lasers, field effect transistors, photoconductive detectors, and photodiodes) have been fabricated using GaN films. GaN photodiodes have the capability of solar blind UV detection and are capable of fast response time due to high electron mobility (as high as 1000 $cm^2V^{-1}s^{-1}$), which is comparable to silicon.

SiC

SiC is another material that has shown promise for UV detection due to its wide bandgap (E_g = 3.0 eV and 3.2 eV for 6H and 4H phases, respectively) [12]. Various optical devices such as blue LEDs, lasers, and UV photodiodes have been developed from 6H-SiC due to the relative ease of doping this material to form ***p*** and ***n*** layers by ion implantation or epitaxial methods. SiC devices are also capable of high-temperature operation, and the photodiodes have shown high quantum efficiency (>80%) in the 250 to 280 nm region. Low dark current is another attractive feature of these devices.

InI

Indium iodide is a wide bandgap semiconductor (E_g = 2.0 eV) being developed for detection in visible and near-UV region [13]. The resistivity of the material is quite high (>10^{10} Ω-cm) and Schottky diodes

© 1999 by CRC Press LLC

are fabricated using evaporated palladium electrodes. Because of the high resistivity, it is possible to deplete relatively large thickness (0.5 to 1 mm) at low bias (<200 V). One of the unique properties of InI photodiodes is their high quantum efficiency (>70%) in the 300 to 600 nm wavelength region, as shown in Figure 56.11, which in combination with its low dark current makes it attractive for low light level detection applications such as scintillation spectroscopy.

Alloys and Bandgap Engineering

In many instances, required properties are attained by bandgap engineering where two or more semiconductors are alloyed together to create a ***ternary semiconductor***. The use of a ternary semiconductor provides the ability to tune the peak wavelength of a photodiode. When two binary compounds are combined, the resulting ternary material usually has properties that lie between those of the constituent binary compounds. Examples of some alloys developed in this manner include $Hg_xCd_{1-x}Te$ for infrared detection, which is created from HgTe (E_g = 0.14 eV) and CdTe (E_g = 1.45 eV), Si_xGe_{1-x} which is a mixture of Si (E_g = 1.1 eV) and Ge (E_g = 0.7 eV) for infrared and visible detection, and $TlBr_xI_{1-x}$ which is a mixture of TlBr (E_g = 2.7 eV) and TlI (E_g = 2.1 eV) for visible detection. A discussion of some recent novel materials that are being developed is presented in the following section and a compilation of relevant properties of various semiconductor materials is presented in Table 56.3.

III–V Ternary Materials

Ternary alloys of GaN and AlN (E_g = 6.2 eV), $Ga_xAl_{1-x}N$, are also being investigated to create optimized UV detectors for desired wavelengths. In the ternary compound, the bandgap depends on the material composition or x and varies almost linearly from 3.4 to 6.2 eV. Such bandgap engineering is desirable to create material with required photoresponse. These devices are also expected to be capable of high

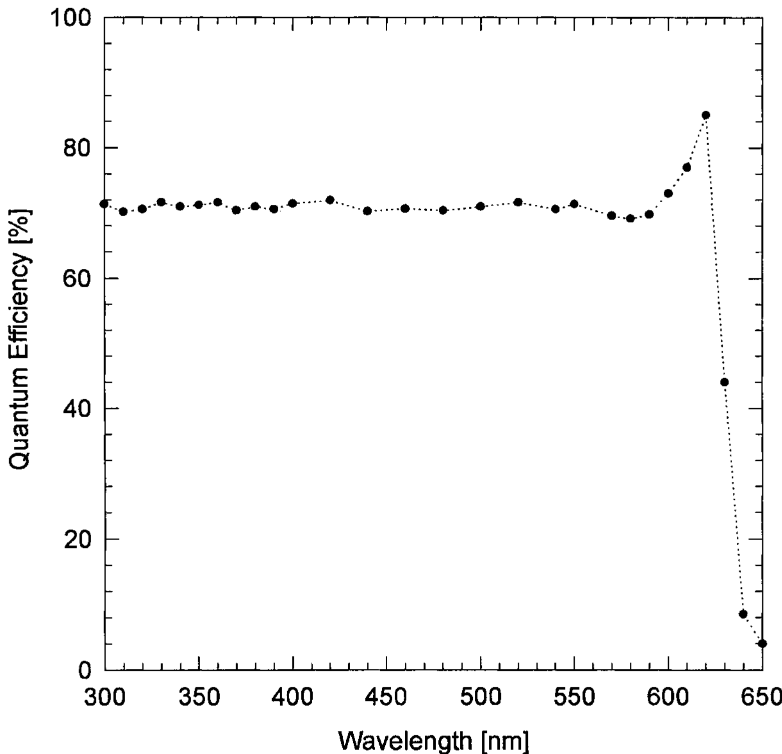

FIGURE 56.11 Quantum efficiency of an InI photodiode. The QE peaks at over 80% near the band edge and has a spectral sensitivity of about 70% into the near-UV.

© 1999 by CRC Press LLC

TABLE 56.3 Properties of Semiconductor Materials Used for Construction of Photodiodes at 25°C

Material	Bandgap	Dielectric constant	Resistivity (Ω-cm)	Electron mobility (cm^2/Vs)	Electron lifetime (s)	Hole mobility (cm^2/Vs)	Hole lifetime (s)	μτ(e) (cm^2/V)	μτ(h) (cm^2/V)
HgTe	0.14	6.4		22000		100			
InAs	0.36	12,5		30000		240			
Ge	0.67	16	50	3900	$>10^{-3}$	1900	1×10^{-3}	>1	>1
Si	1.12	11.7	$\leq10^{4}$	1400	$>10^{-3}$	480	2×10^{-3}	>1	≈1
InP	1.35	12.5	10^{7}	4600	1.5×10^{-9}	150	$<10^{-7}$	4.8×10^{-6}	$<1.5\times10^{-5}$
GaAs	1.43	12.8	10^{7}	8000	10^{-8}	400	10^{-7}	8×10^{-5}	4×10^{-6}
CdSe	1.73	10.6	10^{8}	720	10^{-6}	75	10^{-6}	7.2×10^{-4}	7.5×10^{-5}
a-Si	1.8	11.7	10^{12}	1	6.8×10^{-9}	.005	4×10^{-6}	6.8×10^{-8}	2×10^{-8}
InI	2.01	26	10^{11}					7×10^{-5}	
HgI_2	2.13	8.8	10^{13}	100	10^{-6}	4	10^{-5}	10^{-4}	4×10^{-5}
SiC	2.2								
TlBrI	2.2–2.8		10^{10}					9×10^{-5}	
GaP	2.24								
a-Se	2.3	6.6	10^{12}	.005	10^{-6}	0.14	10^{-6}	5×10^{-9}	1.4×10^{-7}
PbI_2	2.32		10^{12}	8	10^{-6}	2		8×10^{-6}	
CdS	2.5	11.6		300		50			
TlBr	2.68	29.8	10^{12}	6	2.5×10^{-6}			1.6×10^{-5}	1.5×10^{-6}
GaN	3.4	12	$>10^{10}$	300–1000					
Diamond	5.4	5.5		2000	10^{-8}	1600	$<10^{-8}$	2×10^{-5}	$<1.6\times10^{-5}$

temperature operation due to the wide semiconducting bandgap of the material. Similar devices are also been studied from GaP (E_g = 2.1 eV) and AlP (E_g = 2.9 eV) for visible and near UV detection.

Another example is indium gallium arsenide, which is a mixture of InAs (E_g = 0.36 eV) and GaAs (E_g = 1.43 eV) and has been recently commercialized as an infrared detector material in the 1000 to 1700 nm region. InGaAs photodiodes in ***p-n*** diode, ***p-i-n*** diode, and avalanche photodiode configurations are available. InGaAs photodiode arrays coupled to amorphous silicon TFTs are being developed for large area infrared imaging. Other ternary III–V materials that have been investigated for similar reasons include GaAsP, GaNP, and BNP.

Heterojunction Photojunction Detectors

A heterojunction is a junction that exists at the interface of two different semiconductors. This concept can be exploited to produce photodiodes with unique properties such as tuned optical response in the region of interest (by adjusting the composition), and reduced optical absorption at the entrance (by irradiating the wider bandgap semiconductor that is transparent to the optical signal). A number of optical sensors have been fabricated using the heterojunction concept using mostly III–V compounds that can be tuned in composition to create heterojunctions with similar lattice constants in both the semiconductors. The research in the heterojunction devices has been aided considerably by the progress in molecular beam epitaxy. One unique application of the heterojunction concept is to fabricate detectors that have capability of distinguishing wavelengths above or below a certain level. This has been accomplished using a multilayer device (see Figure 56.12) that consists of two layers of $Ga_xIn_{1-x}As_yP_{1-y}$ which have different composition and, therefore, different bandgaps. The layer Q1 has a larger bandgap than Q2 and both are grown on InP. The optical response of this device when irradiated through the InP substrate is shown in Figure 56.12 and shows minimal overlap in the desired bands indicating successful wavelength discrimination.

© 1999 by CRC Press LLC

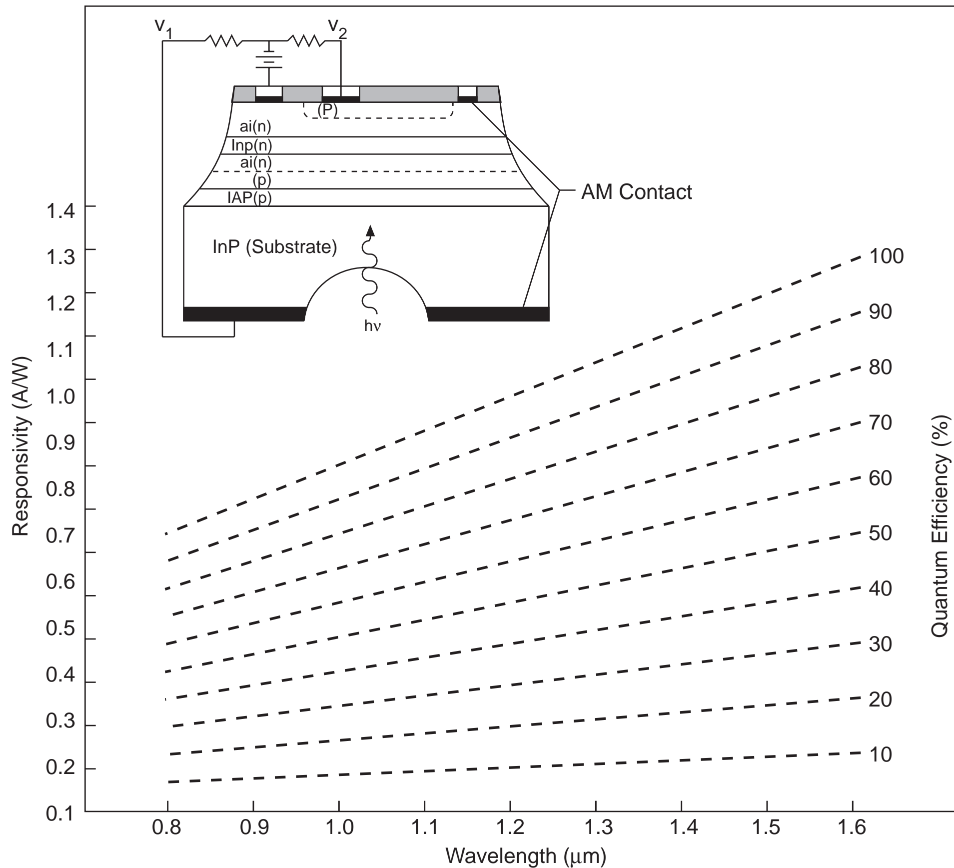

FIGURE 56.12 Responsivity and quantum efficiency of a heterojunction photodiode versus wavelength. The insert shows the cross section of the photodiode

Defining Terms

Bandwidth, B: The range of frequencies over which the photodiode operates.

Breakdown voltage, V_b: The reverse bias voltage at which the applied field overcomes ability of the junction to block current and the device acts like a resistor. The reverse leakage current increases abruptly near this voltage.

Dark current, or reverse leakage current, I_d: The leakage current through the device when at the operating voltage with no incident signal.

Depletion region thickness: The depth of the depleted portion of the diode when at the operating voltage. Photodiodes are frequently operated fully depleted.

Junction capacitance, C_j: Capacitance of the photodiode which decreases as the depletion width increases.

Noise equivalent power, NEP: The incident power that generates a signal equal to the noise, i.e., signal-to-noise ratio (S/N or SNR) equals 1.

Operating bias: The applied voltage at which the device operates.

Peak wavelength: The wavelength with the highest quantum efficiency.

Quantum efficiency, η or QE: The efficiency of converting photons incident on the photodiode into electrons that are detected. Reflection of light from the surface and loss of electrons in the semi-

© 1999 by CRC Press LLC

conductor reduce the efficiency. Reflection losses can be minimized using an antireflection coating on the surface of the device.

Responsivity, (amps/watt): A measure of the signal current produced as a function of the optical power incident on the photodiode.

Spectral response: The quantum efficiency as a function of wavelength.

References

1. S.M. Sze, *Semiconductor Devices: Physics and Technology*, New York: John Wiley & Sons, 1985.
2. *Laser Focus World Buyers Guide,* Pennwell Publishing Co., Nashua, NH, 1997.
3. *Photonics Buyers Guide,* Laurin Publishing Co., Pittsfield, MA, 1997.
4. R.A. Street, Amorphous Silicon Sensor Arrays for Radiation Imaging, *Mat. Res. Soc. Symp. Proc.*, 192, p. 441, 1990.
5. R.A. Street, R.B. Apte, D. Jarad, P. Mei, S. Ready, T. Granberg, T. Rodericks, and R.L. Weisfield, *Amorphous Silicon Sensor Array for X-Ray and Document Imaging*, presented at the Fall Meeting of Materials Research Society Boston, December 1997 and submitted for publication in *Materials Res. Soc.* 478 (1998).
6. K. Shah, L. Cirignano, M. Klugerman, K. Mandal, and L.P. Moy, *Characterization of X-Ray Imaging Properties of PbI_2 Films,* presented at the Fall Meeting of Materials Research Society Boston, December 1997 and submitted for publication in *Materials Res. Soc.* 478 (1998).
7. E. Gatti and P. Rehak, *Semiconductor Drift Chamber on Application of Novel Charge Transport Scheme*, Nucl. Inst. and Meth., A225, p. 608, 1984.
8. R. Farrell, K. Vanderpuye, L. Cirignano, M.R. Squillante, and G. Entine, *Radiation detection performance of very high gain avalanche photodiodes*, Nucl. Inst. and Meth., A353, p. 176, 1994.
9. R.H. Bube, *Photoelectronic Properties of Semiconductors*, Cambridge, UK: Cambridge University Press, 1992.
10. J.I. Pankove, *Optical Processes in Semiconductors*, New York: Dover Publications, Inc., 1971.
11. M.A. Khan, J.N. Kuznia, D.T. Olson, M. Blasingame, and A.R. Bhattarai, *Schottky barrier photodetector based on Mg-doped p-type GaN films*, Appl. Phys. Lett. 63(3), p. 2455, 1993.
12. J.A. Edmond, H.S. Kong, and C.H. Carter, Blue LEDs, UV photodiodes and high temperature rectifiers in 6H-SiC, *Physica B* 185, p. 453, 1993.
13. K.S. Shah, P. Bennett, L.P. Moy, M.M. Misra, and W.W. Moses, Characterization of indium iodide Detectors for Scintillation Studies, *Nucl. Inst. Meth., A,* 380(1–2), 215–219, 1996.

56.3 Charge-Coupled Devices

J.A. Nousek, M.W. Bautz, B.E. Burke, J.A. Gregory, R.E. Griffiths, R.L. Kraft, H.L. Kwok, and D.H. Lumb

Introduction

Use of CCDs for Precision Light Measurement

Charge-Coupled Devices (CCDs) have become the detector of choice for sensitive, highly precise measurement of light over the electromagnetic spectrum from the near-IR (<1.1 μm) to the x-ray band (up to 10 keV). Key advantages of CCDs over their predecessors (photographic emulsions and vacuum tube, electron beam readout devices such as Vidicons and SIT tubes) are high quantum efficiency, high linearity, large dynamic range, relatively uniform cosmetic response, low noise, and intrinsically digital image capture.

© 1999 by CRC Press LLC

CCDs were initially designed as serial data storage media (an electronic analogy to the magnetic Bubble Memory units) in which charge packets were injected into linked capacitors to store data, and read back by moving the packets back out of the device. When it was found that charge packets could be directly induced in the capacitors by exposing them to light, the CCD as light sensor was born.

Physically, ***CCD operation*** consists of four critical stages. First, an incident light photon must be photoabsorbed in the sensitive portion of the CCD chip (called the ***depletion region***). At optical and infrared wavelengths, the absorption results in a single electron being promoted into the conduction band (leaving a hole in the valence band); at shorter wavelengths, the photon has enough energy to make additional electrons via secondary ionizations by the photoelectron.

Second, the photon-induced electrons must be collected, via an electric field within the silicon, into localized regions near the front surface of the chip. The electric field is shaped by implanted dopants and by electric potentials applied to thin conducting strips (***gates***) that prevent the electrons from diffusing away. The resulting charge distribution corresponds to an electronic analog of the light intensity pattern shone on the CCD. The resolution of this pattern is governed by the size of the potential wells, which are designed to be periodic. Each well is called a ***pixel*** and corresponds to the minimum picture element detected by the CCD.

Third, after exposure is completed, the CCD charge pattern must be transferred out of the CCD. This is accomplished by modulating the potential applied to the CCD gates in such a way that no charge packets are mixed, but that each packet moves into the next pixel. The end pixel is transferred into a special pixel array called the ***serial register.*** Each movement of charge resulting from gate potential changes is called a clock cycle, and the serial register receives many clock cycles for each cycle of the full pixel array. The net result is a sequence of charge packets emerging from the serial register, each of which is directly proportional to the amount of light striking a particular location on the CCD.

Fourth, the emerging charges are converted into electric signals by a charge-sensitive preamplifier on the CCD chip. These signals are often digitized by electronics in the camera immediately outside the chip, but analog readouts that produce signals compatible with video standards are also used (the popular hand-held video cameras are examples of this). Research-grade camera readouts are able to measure the charge pulses with accuracies as good as one or two electrons rms, if the CCD and electronics are cooled.

Currently available CCDs carry out these steps so well that they are nearly the ideal detector for precision low light level applications, especially in astronomy. Such an ideal detector would have perfect quantum efficiency (i.e., convert every incident photon into detectable signal), no noise, unlimited dynamic range, linearity in response to incident intensity and position, and completely understandable characteristics.

CCDs have high quantum efficiency because photons interact via photoabsorption in the depletion layer, which directly results in one or more electrons promoted into the conduction band of the silicon lattice, and are very efficiently collected by the CCD. The main obstacles to perfect quantum efficiency are absorption of photons by the gate and insulator materials before they ever reach the depletion regions (or optically, by reflection off the front surfaces) or if the photon passes entirely through the depletion region without interacting.

There are many approaches to enhancing ***CCD quantum efficiency*** for various applications. In soft x-ray and ultraviolet wavelengths, the gate and insulator layers on the front of the CCD absorb too much light. To solve this, CCDs are built with thin gates or thinned substrates and back-side illumination. CCDs are also coated with phosphor coatings that down-convert ultraviolet light to longer wavelengths where the gate transmission is higher.

At hard x-ray and infrared wavelengths, too much light can pass through the depletion region without interacting at all. The depletion region is the part of the CCD pixel that is swept clean of free charges during the readout process. The depletion region gets deeper if higher purity silicon is used, and if higher voltage biases are applied during the readout.

Above 1.1 μm, photons do not have sufficient energy to promote electrons into the silicon conduction band, so other materials, such as germanium or a compound semiconductor such as InAs, InSb, or HgCdTe must be used.

© 1999 by CRC Press LLC

CCD noise results from four major factors: (1) thermal background noise, (2) charge transfer imperfections, (3) charge-to-voltage amplification noise, and (4) cosmetic imperfections in the CCDs due to, for example, microscopic shorts in the insulating layers of the CCD. Factor (1) results from a "dark current" of thermally excited electrons that accumulate in the pixels and can be eliminated by cooling the CCD (typically to –60 to –120°C). Factor (2) results from traps that hold electrons long enough to shift them into following charge packets identified with other pixels. Factor (3) is a fundamental limit related to the temperature and capacitance of the output mode (***kT/C***), but it can be suppressed by signal processing techniques such as "correlated double sampling" to the equivalent of a few electrons (1–5 in state-of-the-art cameras). Factors (2) and (4) can be greatly reduced by improved manufacturing technique, especially scrupulous contamination control during the process.

CCD dynamic range is set by the maximum charge packet that can be stored in a pixel. Termed "full-well capacity," this is set by the depth of the potential well. When the full-well capacity is exceeded, the image of a point source "blooms" as a result of charge leaking into surrounding pixels, and a trail of brighter pixels forms in the readout direction of the CCD due to charge incompletely transferring from pixel-to-pixel during a clock cycle. Modern CCDs have full-well capacities in excess of 10^5 electrons and can be designed even larger. (Note that larger full-well also requires larger output capacitance, so a trade-off is generally required between blooming and low noise.)

CCD linearity in intensity response and position response is very good because the conduction band in the CCD has so many states that the very small injected photocharge does not affect subsequent photon interactions. The position linearity results from the photolithography of the manufacturing process, which must be accurate to less than 1 μm. The primary limitation on linearity results from imperfect ***charge transfer efficiency*** (CTE) in the process of clocking charge packets from pixel to pixel. At readout rates below 100,000 pixels per second, CTE imperfections have four causes.

1. Design imperfections: errors in CCD design can leave potential minima that are incompletely drained during clocking.
2. Process-induced traps: random cosmetic defects, presumably due to imperfections in manufacturing.
3. Bulk traps: lattice defects or impurities that introduce local potential minima, which temporarily capture electrons long enough to remove them from the original charge packet, but re-emit them later.
4. Radiation-induced traps: similar to (3) but resulting from lattice defects caused by low-energy protons. This damage is most commonly seen by spacecraft CCD cameras.

CCD Operation and Data Reduction

In order to achieve ultimate ***CCD performance*** for a given goal, the CCD camera can be operated in special ways, and the postcamera data reduction can be optimized. Typical optical use of CCDs involves timed exposures, where the CCD pixels are exposed to light and the total charge integrated in pixels for a preselected time. At the conclusion of the integration, a shutter closes and the CCD is read out. As noise reduction limits the readout to roughly 100 kpixels/s, a large CCD (2048 × 2048 pixels) readout can take many seconds to complete.

To avoid the deadtime associated with the closed shutter, some CCDs are made with framestore regions. The framestore is a pixel array equal to the integration region which is permanently blocked by a cover from any additional light. The pixels containing the charge pattern resulting from the integration are very rapidly clocked into the framestore region (typically requiring much less than 1 s) and then slowly clocked out into the readout region without moving the integration pixels.

Operationally, CCD reduction requires calibration exposures. These include bias frames, which are readouts with the same integration time but no light striking the CCD, and flat field frames, which have a uniform illumination over the CCD. The bias frames are subtracted from the data frames to set the zero-point corresponding to zero incident radiation. (Note that CCDs will accumulate charge due to thermal electrons and low-level shorts in the gates, even if no light hits the CCD.) The flat field allows

© 1999 by CRC Press LLC

correction for pixel-to-pixel sensitivity variations. Proper flat fielding can remove variations of arbitrary amplitude and spatial scale.

The CCD dark current bias can be reduced by cooling the CCD, or by operating it in an inverted phase mode. In inverted phase operation, the gate electrode is given a suitable negative bias that attracts hole carriers to the front surface of the CCD. These holes fill interface states at the Si–SiO_2 boundary between the conducting depletion region and the insulating layer under the gates. Suppression of these interface states dramatically lowers the dark current because the interface states are much more efficient at thermal electron promotion to the conduction band than the bulk material. Not all phases can be operated in inverted mode in a normal CCD because, without the restraining potentials provided by gates held at positive voltage, the pixel charge packets can intermingle. A special CCD called an MPP (multiphase pinned) device has extra implant doping that isolates the pixels even with all three phases inverted, yielding dark current so low that integration times up to minutes become possible in room-temperature MPP CCDs.

Other important uses of CCDs include cases where the CCD is continuously clocked, without any shutter. Suitable for high light level conditions, the effective integration time becomes the time to transfer a pixel charge across the source point spread function on the CCD. This allows sensitive timing of source intensity changes.

A similar technique is called ***drift scanning,*** where the rate of clocking of pixels equals the rate of motion of the target across the CCD. Such a condition is common in astronomy, where a fixed detector on the Earth sees slow motion of stars in the field of view due to the Earth's rotation.

Drifts and instabilities in the camera electronics can be corrected using a technique called "overclocking." If the serial registers are clocked more times than there are physical pixels in the CCD, then the excess clocks will produce charge pulses corresponding to zero input light and zero dark current. The distribution of the overclock pulse is then a measure of the readnoise of the CCD chip-camera system, and the mean of the distribution sets the zero point of the energy to output voltage curve. Frequently, CCD cameras subtract the mean of the overclock pixels from all output values in a row (called "baseline restoration").

CCD Signal-to-Noise Ratios (SNR)

To see how these characteristics of the CCD relate to measurement, it is instructive to study the SNR predicted for a given exposure time. In a single pixel illuminated by a source that contributes S_o counts (electrons) to the pixel, one also sees contributions from dark current (S_d) and background illumination (S_s, usually called the "sky" in astronomical usages), all in units of counts per pixel per second. The source contribution (S_o) can be expanded into the intensity of light from the source, I; the quantum efficiency of the CCD, Q; and the integration time, t; to provide

$$S_o = I \times Q \times t \qquad (56.17)$$

The camera readout contributes a randomly distributed but fixed Gaussian noise with variance N_r. The SNR of a particular pixel is then:

$$SNR = I \times Q \times t = (I \times Q \times t + N_r^2 + S_d + S_s)^{1/2} \qquad (56.18)$$

If the light from a source is distributed over a number of pixels, n [as might arise from a star viewed through a telescope with a point spread function (PSF) covering n pixels], then if the integral of S_o over the PSF is C_o, and the integral of S_s over the pixels is C_s, then

$$SNR = C_o^{1/2}/(1 + C_s C_o + n + r^2 C_o)^{1/2} \qquad (56.19)$$

Clearly, high Q and low r are desirable, and t should be chosen to make C_o greater than both C_s and r. It is worth noting that, in most optical applications (except for extremely faint sources), it is the

© 1999 by CRC Press LLC

uncertainty in the flat fielding (i.e., the corrections made for pixel-to-pixel sensitivity variations and background) that ultimately limits the achievable SNR.

CCD Structure and Charge Transport

CCD structure and its potential profile under bias

A CCD is a semiconductor device operating under the principle that charges can be temporarily stored and transported along a string or array of MOS capacitors. The basic storage unit is called a pixel and is made up of several MOS capacitors. In almost all CCDs, charges are stored either directly at the oxide–semiconductor interface (surface-channel device), or deeper within an epitaxial layer (buried-channel device). Theoretically, a surface-channel CCD has a larger charge capacity, but it also is prone to noise arising from interface states at the boundary.

The CCD is operated by varying voltages applied to the surface electrodes. Typically, the CCD is kept for a long period in an integration state, where photon-induced electrons accumulate in the potential wells under the CCD pixels. After the integration finishes, the voltages are changed to transport the charge from one capacitor to the next. This sequence of moving charge packets by potential clocking is sometimes called "bucket-brigade" charge transfer.

The storage unit of the CCD is the MOS capacitor and it is possible to deplete, invert, or form a surface accumulation layer in the MOS capacitor by simply changing the surface potential. CCDs operate in the so-called "deep depletion" mode when the surface layers are fully depleted. For a buried-channel CCD with an ***n***-type buried layer within a ***p***-type epilayer, this would require the application of a positive bias to the surface electrodes. The equations governing the one-dimensional calculations of the potential distribution in the MOS capacitor are [1]:

$$\frac{d^2\psi}{d_x^2} = 0 \qquad -d < x < 0$$

$$\frac{d^2\psi}{d_x^2} = -q \bullet \frac{N_D}{\varepsilon_s} \qquad 0 < x < t$$

$$\frac{d^2\psi}{d_x^2} = q \bullet \frac{N_A}{\varepsilon_s} \qquad t < x < x_p \tag{56.20}$$

where ψ is the potential, N_A is the substrate acceptor density, N_D is the donor density in the epilayer, x_p is the depletion edge in the ***p***-type substrate, and ε_s is the semiconductor permittivity. Note also that d is the oxide thickness and the origin ($x = 0$) is located at the oxide–semiconductor boundary.

The boundary conditions will be:

$$\psi(x = -d) = V_G \qquad \left.\frac{d\psi}{d_x}\right|_{x=t^-} = \left.\frac{d\psi}{d_x}\right|_{x=t^+}$$

$$\varepsilon_{ox} \bullet \left.\frac{d\psi}{d_x}\right|_{0^+} = \varepsilon_s \bullet \left.\frac{d\psi}{d_x}\right|_{0^+} \qquad \psi(x = t^-) = \psi(x = t^+)$$

$$\psi(x = 0^-) = \psi(x = 0^+) \qquad \psi(x = t + x_p) = 0 \tag{56.21}$$

© 1999 by CRC Press LLC

and the solutions are:

$$\psi = V_G - E_{ox} \bullet (x+d) \qquad -d < x < 0$$

$$\psi = \psi_{max} - q \bullet N_D \bullet (x - x_n)^2/(2\varepsilon_s) \qquad 0 < x < t$$

$$\psi = q \bullet N_A \bullet (x - t - x_p)^2/(2\varepsilon_s) \qquad t < x < t + x_p \tag{56.22}$$

where E_{ox} is the electric field in the oxide layer, V_G is the gate bias voltage, and x_n is the position of the potential maximum.

Figure 56.13 shows a typical potential profile across the MOS capacitor in a buried-channel CCD. Note the presence of a potential maximum, ψ_{max}, where the electrons will reside. It is given by:

$$\psi_{max} = \psi_J \cdot (1 + N_A/N_D) \tag{56.23}$$

where $\psi_J = q \bullet N_A \bullet x_p^2/(2\varepsilon_s)$. Since x_p increases linearly with N_D, the potential maximum ψ_{max} and hence the charge storage capability also increases for a heavily doped epilayer. The derivation of the potential profile in a surface-channel CCD will be similar, but with d set to zero.

Charge Transport

Charge transport in a CCD refers to the transfer of charges along the MOS capacitors (i.e., from one pixel to the next). There are several clocking schemes used, generally divided according to how many external voltage regions are applied per pixel, ranging from one (uni-phase) to four-phase.

Computation of charge transport in a CCD requires solving the two-dimensional Poisson equation with appropriate boundary conditions to obtain the potential distribution within the pixel for each separate phase within the clocking cycle. Numerical techniques using finite-difference or finite-element methods have been used. For charge transfer in an n-type epilayer, the electron flux, $F(x)$, is given by:

$$F(x) = n_s(x, t) \cdot \upsilon(E(x)) - D(E(x)) \cdot (n_s(x + \Delta x, t) - n_s(x, t)) = \Delta x \tag{56.24}$$

where $n_s(x, t)$ is the electron density, $E(x)$ is the electric field in the x-direction, $\upsilon(E(x))$ is the field-dependent velocity, and $D(E(x))$ is the electron diffusivity. Figure 56.14 shows the time evolution of charges along a CCD. Some "smoothing" of the output charge profile is often observed and, for high-

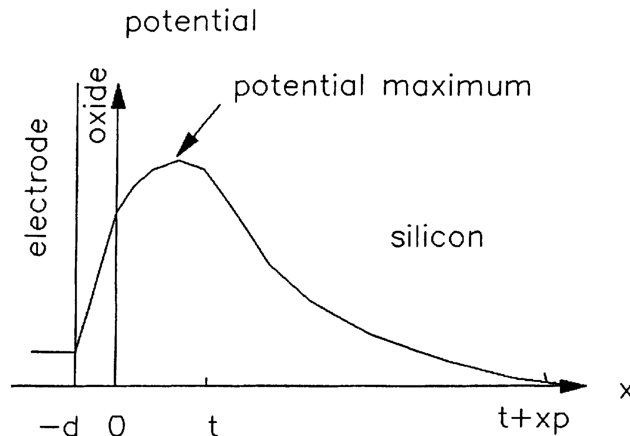

FIGURE 56.13 Potential profile across MOS capacitor.

© 1999 by CRC Press LLC

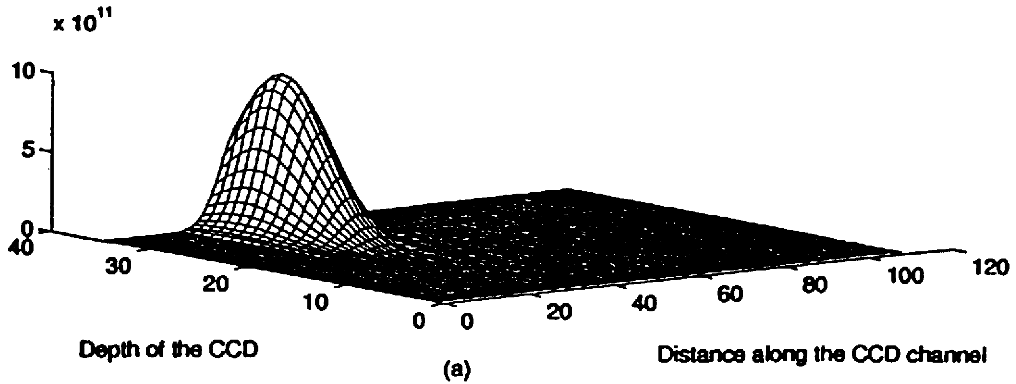

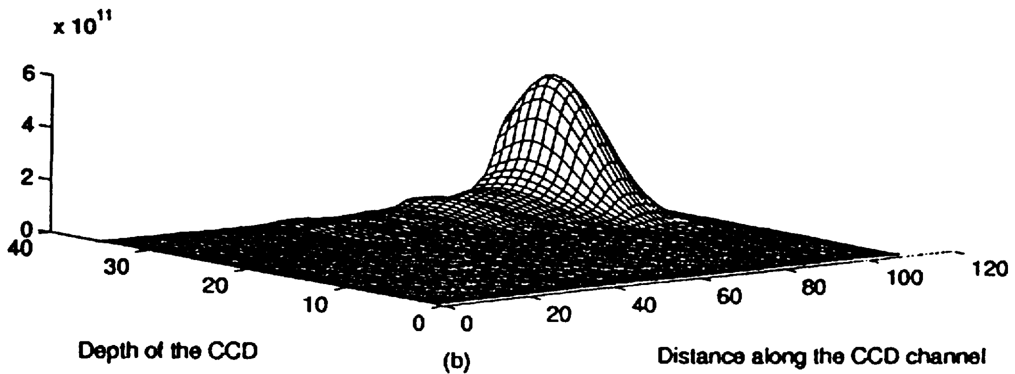

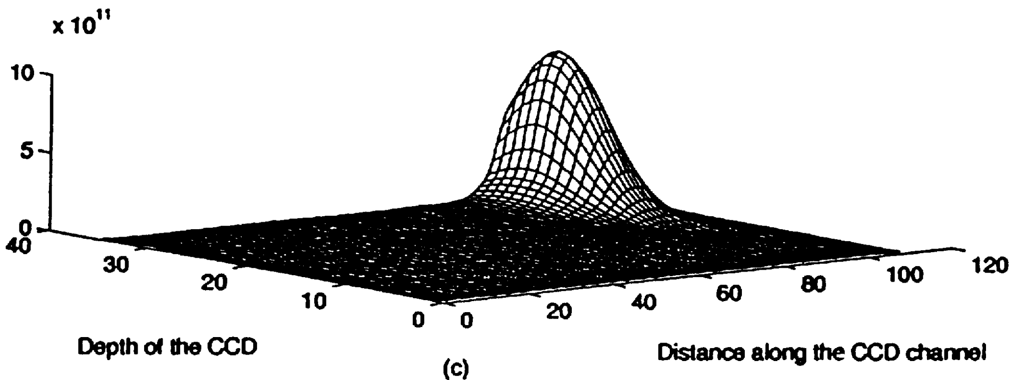

FIGURE 56.14 Time evolution of charges along a CCD: (a) t = 200 ps; (b) t = 400 ps; (c) t = 600 ps.

speed devices, velocity saturation will be important. Computations of charge transfer are sometimes carried out using a equivalent circuit model for the CCD in a SPICE-type simulator. It has been shown to offer both faster computation time and the ability to include external support circuits into the model.

Charge transfer efficiency, η, is the key figure-of-merit in a CCD, at least comparable to quantum efficiency. A common technique to determine η is to measure the amplitude response of the CCD using a network analyzer. η is then related to the amplitude response of the output, G_V through the following relationship:

© 1999 by CRC Press LLC

$$G_V = \exp\{-N_T \bullet (1-\eta) \bullet [1-\cos(2\pi f/f_c)]\} \quad (56.25)$$

where N_T is the number of transfers, f is the signal frequency, and f_c is the clock frequency. For the relatively mature Si CCD technology, charge transfer efficiency of 0.99999 can be easily achieved. Note, however, that this analysis applies to sinusoid illuminated scenes and test signals, but does not apply to delta function injections of charge that are infrequently transferred, as applies to the x-ray photon-counting case.

Input and Output Structures

The input structure of the CCD usually consists of a ***p-n*** junction and two or more input gates as shown in Figure 56.15. Initially, when the input voltage, V_{id} is pulsed low, charges will flow through the input (electrode) into the potential well created under the input gates G_1 and G_2. When V_{id} returns to its equilibrium value, charges will be withdrawn except those residing in the potential well formed by the potential difference between G_1 and G_2. Charge injection is now complete and a drop in the potential Φ_1 at the transfer gate will allow charges to enter into the first CCD pixel. The input charge, Q_{in}, is approximately given by:

$$Q_{in} = C_{ox} \cdot (V_{G1} - V_{G2}) \quad (56.26)$$

where C_{ox} is the oxide capacitance, and V_{G1} and V_{G2} refer to the voltage difference between G_1 and G_2. In CCD sensors and detectors, signal input normally relies on the incident photons liberating charge within the depletion region (after traversing either the front gates [front-illuminated] or the back surface [back-illuminated]). Charges so created will be collected in the potential wells formed by the clock voltages.

Normally, the output structure of the CCD consists of a reset switch and a floating diffusion (FD) or floating gate (FG) amplifier. These are shown in Figure 56.16. During sampling, the output charge flows into the floating node and a voltage is developed across the output capacitance, which is a combination of the depletion capacitance of the floating node and the input gate capacitance of the source follower. In general, the voltage output, V_{sig}, can be expressed as:

$$V_{sig} = Q_{inj} \cdot A_V / C_{fd} \quad (56.27)$$

where Q_{inj} is the injected charge, A_V is the small-signal voltage gain of the output amplifier, and C_{fd} is the capacitance between the floating node and ground. Since both A_V and C_{fd} are sensitive to the output

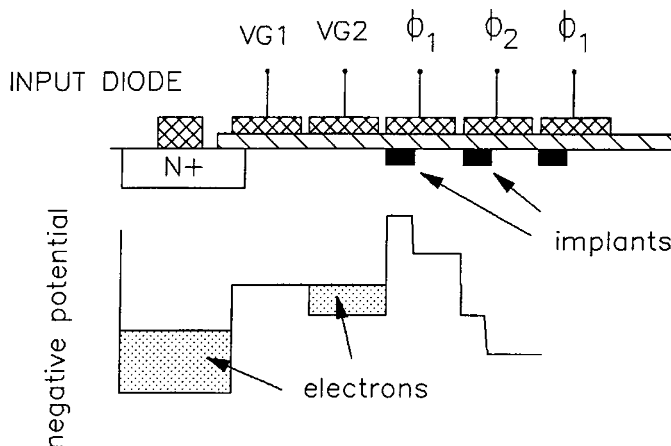

FIGURE 56.15 Input structure of a CCD.

© 1999 by CRC Press LLC

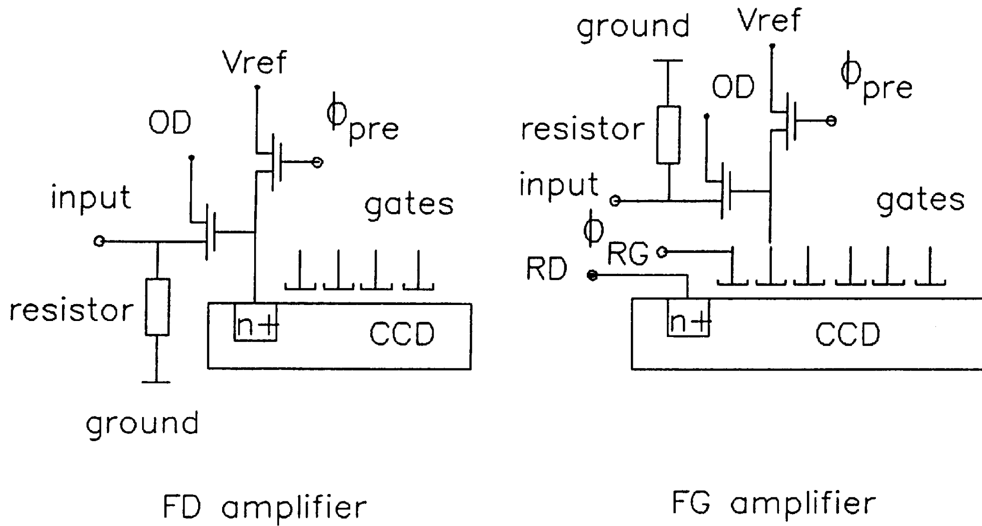

FIGURE 56.16 Output structures of a CCD.

charge and temperature, this type of output structure is not generally linear. Improvements in the output structure can be achieved using either a floating gate amplifier or Miller feedback at the output to reduce parasitic capacitances.

Noise in CCDs

CCD noise will degrade the SNR. The following are important noise sources in CCDs:

1. Thermal noise, or dark current, is due to thermally excited electrons that accumulate in the pixels during the integration. In applications where the clocking time is short compared to the integration time, the equivalent noise election, n_{th}, is given by:

$$n_{th} = \sqrt{J_d \bullet A_E \bullet t_{int}} \tag{56.28}$$

where J_d is the leakage current density, A_E is the area of the transport electrode, and t_{int} is the integration time. A lowering of the operating temperature will normally reduce the leakage current density and hence the equivalent noise electron.

2. Bulk traps are the dominant noise sources for buried-channel CCDs and the equivalent noise electron from this source is:

$$n_{trap} = \sqrt{N_t \bullet V_{sig} \bullet Nt \bullet e^{-T_t/\tau_e}[1 - e^{-T_t/\tau_e}]} \tag{56.29}$$

where V_{sig} is the volume of the charge packet under the transfer electrode, N_t is the density of the bulk trap states, T_t is the transfer time, and τ_e is the electron emission time constant. It can be observed that the equivalent noise electron increases as the size of the charge packet increases, an indication that bulk traps do not generally affect the SNR in CCDs. In x-ray photon counting applications some effects of bulk trapping noise have been seen.

3. Both the input and output of a CCD involve charge storage across capacitors that will be affected by fluctuations in the circuit. The equivalent noise electron for this process is:

$$n_{inp} = \sqrt{kT \bullet C_{inp}} \quad n_{out} = \sqrt{kT \bullet C_{out}} \tag{56.30}$$

© 1999 by CRC Press LLC

where kT is the thermal voltage and C_{inp} and C_{out} are the input and output capacitances. A special signal processing technique known as "correlated double sampling" can be used to reduce this kTC noise at the CCD output.

1/f noise is also present in the output amplifier and is only significant at low frequencies. Methods to reduce 1/f noise include multiple sampling using distributed floating-gate amplifiers (DFGA) [2] and noise cancellation techniques using alternate gain inversion (AGI) [7].

4. The maximum SNR of a CCD is limited by the maximum amount of charge that can be stored in a pixel, divided by the equivalent noise electron. Expressed in decibels, it is:

$$\mathrm{SNR} = 20 \log(Q_{max} = Q_{noise}) \tag{56.31}$$

The maximum charge is:

$$Q_{max} = C_e \cdot \psi_{BH} \tag{56.32}$$

where C_e is the depletion capacitance associated with the electrode, and ψ_{BH} is the depth of the potential well.

CCD Power Dissipation

CCD power dissipation is primarily linked to the charging and discharging of the gate capacitances. This power is mainly consumed by the clock driver and is given by:

$$P_{clock} = C_c \cdot V^2 \cdot f_c \tag{56.33}$$

where C_c is the clock line capacitance associated with the electrodes, V is the clock voltage, and f_c is the clock frequency. For f_c = 100 MHz and V = 5 V, typical values of P_{clock} are 50 μW per pixel.

In addition to P_{clock}, the on-chip power dissipation per pixel is approximately given by:

$$P_{CCD} \approx nq(f_c L)^2/\mu_e + 2nqf_c(\psi_{BH} - nq/(2C_e) \tag{56.34}$$

where n is the number of electrons in a pixel, L is the pixel length, and μ_e is the electron mobility. The overall power dissipation in a CCD is therefore the sum of P_{clock} and P_{CCD}.

CCDs Applications to Light Sensing

Optical Imaging and Spectroscopy

The many fine properties of CCDs have made them the detector of choice for the recording and readout of images at both high and low light levels. The applications include (1) reconnaissance, both civilian and defensive, (2) scene and personnel monitoring, (3) robotics, and (4) astronomy. In astronomy, CCD cameras have found their way into almost all observatories in the world, both for direct readout of images and as the readout cameras for spectrographs.

Perhaps the most exacting application of CCDs has been to astronomy, a discipline in which the characteristics of the CCD need to be pushed to their limits in order to gain the optimum performance. As well as the attempt to optimize this performance in order to gain as much science as possible from the images, it has also been crucial to calibrate the devices as precisely as possible and to fully understand their behavior. In this sense, astronomy has been the "driver" for the scientific development of CCDs. Large-scale commercial applications, such as video recorders, monitoring cameras, etc., have driven the need for improved manufacturing yield, blemish-free operation, uniformity in performance, and reliability.

In order to illustrate the importance of CCDs to exacting scientific requirements, this section will focus largely on the applications to astronomy.

© 1999 by CRC Press LLC

The early demonstration of the performance of a commercial CCD at the focus of a telescope quickly led to the realization of their potential for both space and ground-based astronomical cameras and instruments. Fortunately, this development in the early 1970s was just in time for the first major optical observatory in Earth orbit, the Hubble space telescope (HST). Perhaps the most spectacular application of CCDs to visible light imaging has been within the cameras on board this telescope, i.e., the wide field and planetary cameras built at the Jet Propulsion Laboratory. The CCDs in these cameras consisted of 800×800 pixel arrays, with each pixel of size 25 μm. The first version of this camera contained eight thinned, back-illuminated devices that were more or less fully depleted. An accumulation layer at the back surface was achieved by flooding the devices with UV light from a lamp internal to the instrument. This accumulation layer allowed the collection of charge resulting from the photoelectric absorption of blue light, and accelerated the charge to the frontside potential wells. Furthermore, the devices were coated in a down-converting coronene phosphor that converted UV light into the yellow-green wavelength band, thus allowing a 20% efficiency in the UV. These devices thus had relatively high quantum efficiency from the UV through to about 1 μm, vitally important for an instrument collecting photons from galaxies billions of light years away in the universe. As well as their high quantum efficiency, these devices had high charge transfer efficiency and relatively low readout noise at the time of their development. All of these characteristics have since been superseded—at first by an improved version of the camera installed in the HST in late 1993, and then in the Advanced Camera for Surveys, to be installed in 1999. These later instruments had larger format, higher quantum efficiency, and lower readout noise. During the 1980s, devices were developed with these large formats and with readout noise levels approaching one electron.

Starting with modest arrays of size on the order of a few hundred pixels in the 1970s, the devices that became available in the 1990s were as large as 4096 pixels square. As well as in space, these devices have been employed at the prime foci of the world's largest telescopes to give images covering more than 10 arc minutes on a side while still sampling the atmospheric-limited resolution (arcsecond or subarcsecond) adequately. Such devices, when exposed to the sky for up to an hour through a broadband filter, can produce images with tens of thousands of objects for statistical studies in astronomy.

Typical pixel readout rates for astronomical cameras are of the order of 50 kHz, taking tens of seconds for a full readout. Integration times for astronomical CCD cameras can vary from fractions of a second to tens of minutes or even times in excess of an hour, usually limited by the background noise induced by cosmic ray particles and their secondaries. These cosmic ray "events" can be removed by taking at least two frames of data and cross-comparing them. This is important even on the ground, where the radioactive background and muon-induced events total about one per cm^2 per minute; but the cosmic-ray background in space is about one per cm^2 per second, so that camera exposures are rarely longer than 10 to 20 min. Sophisticated computer algorithms have been developed in order to remove the effects of this background radiation.

Of special importance to applications in space research is the packaging of the devices. Contamination of the cold CCD surface by as much as a monolayer of a heavy molecule will effectively render the CCD useless in the vacuum-UV, for example. Careful attention must therefore be paid to the local instrument environment. The CCDs on the HST were in hermetically sealed packages, and the contamination problem was transferred to the lenses covering the CCD packages. In order to achieve optimum performance, the overall camera has to be designed to satisfy the exacting requirements of the CCD, from the point of view of thermal control and stability, absence of electronic interference, and rigorous attention to the elimination of water or heavy molecule contamination. For space application, it may also be advantageous to surround the CCD package with a cosmic-ray shield, such as the 1 cm (0.4 inch) of tantalum used in the CCD cameras on the HST and the Galileo mission to Jupiter. Such radiation shields have to be designed with caution, lest they introduce more secondary particles and induced radioactivity than the primary protons that they stop.

Finally, much effort is put into the processing of astronomical CCD data [24]. Special techniques have been developed to calibrate the pixel-to-pixel nonuniformity in quantum efficiency (a function of wavelength), both on large and small scales. With some effort, this nonuniformity can be calibrated to levels

© 1999 by CRC Press LLC

below 1%. Although it may be easy to expose the CCD to a diffuse source such that there are at least 10,000 electrons per pixel, the corresponding flatfield calibration accuracy may be compromised at low light levels. For astronomical applications, especially in space, most of the pixels may receive only tens of electrons or fewer during an exposure. Low-level traps (including those caused by cosmic radiation) will then manifest themselves in the form of charge-transfer inefficiencies over localized areas or columns. It may be important to calibrate the CCD at the same exposure levels as those typically encountered during the science observation. One way of effecting this is to use hundreds or thousands of frames of data taken in different parts of the sky, and rejecting the astronomical objects in them. These "sky frames" can then be used to produce a "super sky-flat," which is the average of the individual frames of data.

CCD X-ray Imaging Spectroscopy

Scientific applications such as astronomy have been responsible for driving improvements in CCD technology. In the x-ray domain, for example, CCDs are starting to be employed for medical radiography, where the digital imaging capability and high sensitivity allows for lower patient doses and online image processing. As high-resolution readout detectors of dispersive x-ray spectrometers, CCDs are becoming widely used in the new generation of high brilliance synchrotron beamlines. As spectrometers, they are also being considered in some applications as replacement for Si(Li) diodes, where the higher operating temperatures and improved resolution and efficiency down to x-ray energies below 1 keV leads to applications of interest to biological science and technology.

In contrast with optical imaging applications with many photons per charge packet, to measure x-ray spectral information directly with a CCD single photons per pixel per image frame are required. To use the CCD as a nondispersive x-ray spectrometer requires that the correspondence between the magnitude of the electron charge packet generated initially by the x-ray photon, and the signal measured at the CCD output, must be maintained. This places a very stringent requirement on the efficiency of charge transfer. However, even before the process of charge transfer is initiated, the physics of the charge collection may also degrade the energy measurement process.

The absorption process for a photon of energy E begins with the ejection of a photoelectron, of energy $E - E_B$, where E_B is the binding energy of the appropriate silicon atom electron shell. The range of the photoelectron may be only a fraction of 1 μm. In a few percent of cases, a silicon K shell fluorescence photon may be emitted, and this has a range of about 10 μm, so that there is a finite probability of the event energy splitting into more than one pixel.

Eventually, a proportion of the energy is converted to free electrons, the rest into phonons. The average energy to create an electron-hole pair is roughly constant at about 3.6 eV of incident photon energy per pair produced in silicon. If this free electron charge packet is created in the depletion layer of the CCD, it is promptly drifted under the influence of the electric field to the buried-channel collection site. During this drift time (t_d), the charge can laterally diffuse within a radius $\sim \sqrt{2Dt_d}$, where D is the diffusion constant. Except for the charge clouds originating deep in the depletion layer, this radius is small compared with the typical pixel size. If the charge is generated in a field-free layer ***outside*** the depleted volume, it will radially diffuse until a fraction recombines or reaches the depletion layer. The latter fraction then starts to drift with the same additional lateral drift as the depletion layer charge packets.

The pixel boundaries are loosely defined by the asymmetric fields created by electrode biasing schemes and surface channel stop implants, and not hard physical boundaries. Hence, any lateral spreading processes may allow some splitting of the initial charge packet between pixels. Furthermore, charge ***loss*** may be experienced either by the partial recombination of events when liberated deep below the depletion layer, or if the fraction of split charge is too low to be recognized against the device noise level.

In astronomical applications, in space-borne observatories, there is a continuous low-level background of charged particles. Rather than liberating point-like charge clouds, they liberate a population of signal electrons along their tracks throughout the silicon. They may be easily discriminated against x-rays if these tracks are highly skewed with respect to the silicon surface and cross many pixels. Also, if the track is long enough, the magnitude of total charge cloud generated may be large compared with the typical x-ray charge packet.

© 1999 by CRC Press LLC

These features impose a requirement to perform event recognition and analysis. To perform this on-ground would require transmission of all pixel data, including empty pixels, which for megapixel CCD frames generated on second time scales is quite infeasible. Performing this recognition on-board first requires a comparison against some lower threshold. Selection of this level is critical—too high and some split charge may be neglected with a consequent degradation of energy resolution. Too low a threshold, and many spurious events will be counted. If there is a drift or change in the zero-energy signal upon which this threshold is applied, the energy scale may be misregistered, and/or the relative fraction of events selected at different x-ray energies may be unknowingly altered. Simulations show that for the potential energy resolution of CCDs, spectral analysis of cosmic plasmas will demand a calibration of relative detection efficiency versus energy to ~3%. If the threshold value is set at about 4σ times the readout noise, this calibration may be degraded by as little as a single digital bit of a commonly used 12-bit ADC in the CCD readout electronics. Thus, the realtime digital processing of events is required to be fast and complex.

A further complication of the event splitting is that to avoid pile-up in CCD frames, the probability of having multiple events per pixel is made more stringent by requiring surrounding pixels to have no signal, and allow this recognition process. Typically, an event rate of 1 photon per 200 pixels per CCD frame is therefore imposed, but this places a rather low limit on attainable count rate performance. Especially with high-resolution focusing optics of observatories such as AXAF[5], this can be much lower than for many previous experiments. If the core of the point spread function of the mirror is not to be degraded by this effect, then special readout formats that reduce the imaged area, in order to accelerate frame readout times, must be employed.

Future Improvements to CCDs

Backside CCDs

The useful spectral range of conventional CCD detectors, although quite broad, is limited in part by the presence of the polysilicon gates on the front surface. As is illustrated in Figure 56.17, photons with

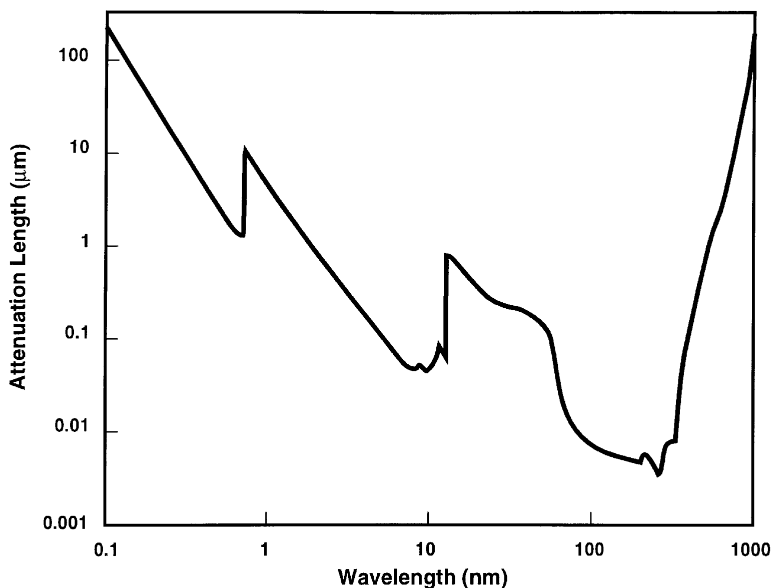

FIGURE 56.17 Attenuation length in silicon in the soft x-ray through near-infrared spectral range. The polysilicon gates of front-illuminated devices, which are typically ~0.4 μm thick, are strongly absorbing at wavelengths for which the attenuation length is less than the gate thickness, viz. wavelengths (~3 mn < λ < ~400 nm). Thin-gate and back-illuminated CCDs, with much thinner dead layers, offer improved detection efficiency in the soft x-ray and UV portions of the spectrum. (From References 8 and 9.)

© 1999 by CRC Press LLC

wavelengths in the range ~3 nm < λ < ~400 nm have attenuation lengths in silicon less than the typical thickness of the gate structure (~0:4 μm). Photons in this spectral range are therefore absorbed before they can enter the photosensitive volume of the detector. For conventional CCDs, the detection efficiency is no more than a few percent in this band. If the gates can be made thinner by an order of magnitude, or avoided altogether, then the detection efficiency can be improved dramatically in both the very soft x-ray and the UV. Efforts following the former approach are described below. The latter strategy, which requires illumination of the back surface of the CCD (that is, the surface opposite the gates) is discussed here.

There are a number of techniques that can be used to produce back-illuminated devices [10–12], but they must all deal with two constraints: lateral diffusion of the photoelectrons before they are captured in the buried channel of a specific pixel and the tendency for photoelectrons to recombine at the back surface of the Si.

The lateral diffusion of electrons can lead to a loss of resolution of the CCD since they may cross the boundary between one pixel and another, leading to an erroneous assignment of the origin of the photon that created the electron. This problem is minimized by thinning the ***back-illuminated CCD*** to thicknesses that are on the order of the depletion depth of the Si, so the least drift occurs before the electron is captured in the potential well of the buried channel. This thinning is accomplished by a combination of methods, including mechanical grinding and polishing and wet etching. Handling of back-illuminated CCDs after thinning, however, is a problem since the remaining Si is between 10 and 100 μm thick, and is not strong enough to support rough handling, or even the intrinsic stresses arising from the initial fabrication of the CCD. To circumvent this problem, rim thinning or frame thinning can be used; in the first case, a rim several millimeters wide around the circumference of the wafer is protected during the thinning process, while in the latter, a region 1 or 2 mm wide around each device is protected.

Lateral diffusion can also be reduced by imposing an electric field through the thickness of the thinned membrane; but if this is done by imposing an electrode on the back surface, then the device will have a reduced QE (quantum efficiency) due to absorption in this layer. The presence of a depletion region in the CCD will also give rise to an electric field, which reduces the lateral diffusion of electrons; but if the desired depletion region is on the order of tens of micrometers, in order to image high-energy x-rays or IR photons, then the induced field will be small, due to the low doping levels in the silicon and Gauss' law.

Although the lateral spread of photoelectrons is a problem, the loss of carriers to recombination at the back surface presents a greater technical difficulty. The recombination velocity can be minimized by introducing a strong electric field at the back surface and by passivating this surface. There are several methods employed to generate this electric field: one is by implanting carriers (***p***-type for the case where photoelectrons are to be captured) and annealing the sample to activate these carriers [11], a second is to deposit a thin layer of metal with the appropriate work function difference (typically Pt or another transition metal) [10], while a third method is to grow a heavily doped epitaxial layer on the back surface [13]. In the implant method, strong electric fields can be generated and the annealing process can help to passivate the back surface, but high-temperature annealing of the wafer can present a problem if metallization is present, unless excimer laser annealing is employed [14]. Deposition of a thin metallic layer can lead to long-term instability of QE and does not appear to yield the highest QEs. Deposition of an epitaxial layer relies on the use of sophisticated equipment and surface cleaning methods.

In addition to introducing an electric field on the back surface, it is necessary to electrically passivate that surface to lower the electron recombination velocity. Again, there are several approaches. The flash gate technique is probably the simplest, relying on inserting the sample in a steam atmosphere, but it is not stable over time [10]. Another method is to grow a high-quality oxide on the back surface [11], but this requires the use of high temperatures, which could melt metalizations and allow any dopant layer to diffuse too deeply into the silicon.

Although the aim of the backside treatment process is always to maximize the fraction of charge collected from the vicinity of the back surface, there are subtle differences in requirements that depend on the application. In the UV (100 nm < λ < 400 nm), the extremely small attenuation lengths (see Figure 56.17) place a premium on nonnegligible (>~50%) charge collection efficiency very close to the back surface. Therefore, in UV sensors, the field in the immediate vicinity of the back surface is extremely

© 1999 by CRC Press LLC

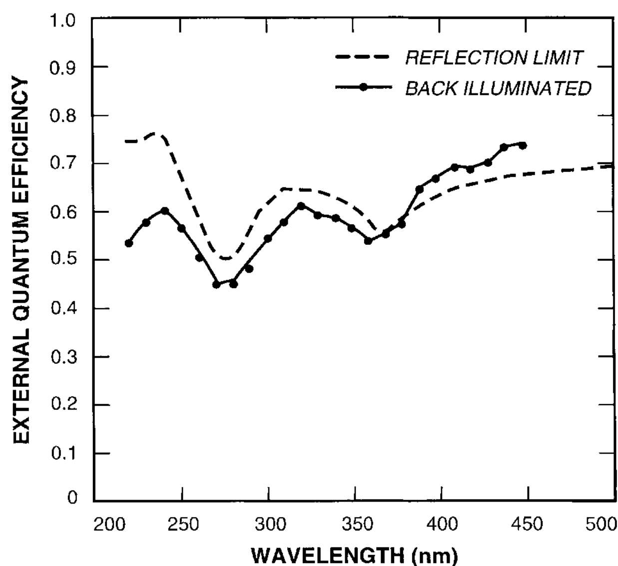

FIGURE 56.18 External quantum efficiency of back-illuminated CCD using an implanted and annealed back side. For comparison purposes, the external quantum efficiency of an ideal detector is shown, after modeling for the antireflection coating present on the back-illuminated detector.

important. Moreover, the real part of the index of refraction of silicon is quite high in the UV and optical bands, and Fresnel reflections limit the external detection efficiency that can be achieved. Thus, significant improvements in the UV response of back-illuminated CCDs have been obtained via the application of antireflection coatings as a part of the backside treatment process [12].

In the very soft x-ray range (2 nm $< \lambda <$ 100 nm), the attenuation length can be larger by a factor of 10 than in the UV. Moreover, the range of the secondary photoelectrons is large enough to be comparable to the attenuation length [15], so the physics of the secondary ionization process becomes important. Thus, in the very soft x-ray regime, it is the average properties of the device over scales of a few hundred nanometers that determine performance. However, for spectroscopic applications, the theoretical limit of device performance cannot be reached unless the charge collection efficiency substantially exceeds ~90%. Thus, in the soft x-ray, one requires very high collection efficiency over a relatively large volume in the vicinity of the back surface.

Any backside fabrication techniques will probably require compromises to be made, but it is possible to achieve very high external QE in the UV, as shown in the accompanying Figure 56.18, and in the soft x-ray region where 77% QE has been achieved at 277 eV [16]. Further improvements are necessary to achieve good results in the vacuum UV and theoretical limits for energy resolution in the soft x-ray. These improvements are possible, but will probably depend on the continued development of sophisticated processing tools.

Thinned Gate CCDs

Recently, a new type of CCD was developed that was optimized for spectroscopy below 1 keV. This detector, called a thin gate CCD (or TGCCD), contained two novel features: floating gate output amplifiers (FGAs or "skippers") and thin gates (electrodes) [2]. The goal was to develop a detector that had Fano-limited energy resolution with nonnegligible QE over the 200 eV to 1000 eV bandpass. This section briefly describes this detector and compares it with more conventional CCDs.

Most conventional CCDs use a floating diffusion amplifier (FDA) to read out the signal charge. The readnoise of the FDA has improved from several hundred electrons (rms) in the 1970s to less than 3 electrons in the last few years [3]. The energy resolution of CCDs over the entire soft x-ray bandpass is now limited by factors other than readnoise. It is desirable to push the readnoise down from a few

© 1999 by CRC Press LLC

electrons to a fraction of an electron because it allows photons of lower energy to be detected in single-photon counting mode.

One method to further reduce the readnoise is to read out the same charge packet multiple times. The signal charge is destroyed when read out through an FDA. In the FGA, however, an insulating gate is placed between the charge transfer channel and the output node. Gates around the output node are used to read out and withdraw the signal charge multiple times. The readnoise is then reduced by the square root of the number of readouts. Effective readnoises of less than 1 electron have been demonstrated using the FGA [2,4], and photons of energy 66 eV (Al L_{α}) have been detected using the TGCCD. If the readnoise could be pushed to a fraction of an electron, it would be possible to detect optical photons in the single-photon counting mode.

Lower Readnoise

The other novel feature of the TGCCD is its electrode structure designed to maximize soft x-ray QE. Most conventional front-side illuminated CCDs have several hundred nanometers of SiO_2/Si_3N_4 insulator and Si electrode on the surface. These layers strongly limit the quantum efficiency of the device below 1 keV, but Fano-limited energy resolution is routinely achieved. The conventional solution to increase the low-energy QE has been to etch away the back surface of the device and illuminate it from behind (a back-side illuminated CCD). The difficulty with this technique is that the energy resolution is seriously degraded due to charge diffusion and poor charge collection.

The thin gate CCD is a front-side illuminated device with a unique gate structure that gives reasonable soft x-ray QE (0.20 at 277 eV), while retaining the good energy resolution of front-side illumination. The detector is a three-phase CCD. The first two phases (comprising only 1/3 of the active area of the device) are covered with 400 nm of polysilicon (or just poly) in the usual way. A third layer of poly is deposited on top of the first two and acts as a bus for a fourth (40-nm thick) layer of poly that defines the third clock phase. Two-thirds of the active area of the detector is therefore covered with only the insulator (100 nm of SiO_2 and Si_3N_4) and this fourth layer of poly. The measured energy resolution of this device is 34 eV at C K_{α} (277 eV). This is approximately a factor of 3 better than the best energy resolution obtained with the ACIS back-side illuminated CCDs [5]. Simulations show that an astrophysical spectrum obtained with TGCCD contains as much or more information than one obtained with a back-side illuminated CCD [6].

Radiation Damage

CCDs are often used in environments in which they are subject to ionizing radiation, and this radiation can degrade their performance. In particular, radiation damage plays an important role in the performance of most space-borne detectors. The Van Allen belts contain protons and electrons with energies of tens of MeV. These particles can produce damage by several mechanisms. Protons can generate vacancy-interstitial pairs in the Si lattice, which diffuse freely, even at cryogenic temperatures, and it is possible for the vacancy to form a complex with P atoms in the *n*-Si buried channel that traps electrons. The trap reduces CTE by preventing signal electrons from leaving the pixel during the clocking cycle. Electrons can also produce vacancies (although with much lower cross-section than the protons), but they can also create dangling bonds at the SiO_2–Si interface above the buried channel, leading to a shift in operating voltage in the CCD and contributing to noise.

The P–V complexes remove electrons from a charge packet in the conduction band of silicon. In the worst-case limit, when the illumination levels are so low that each charge packet transferred encounters each trap in its empty trap state, the degradation of CTE is approximately 5×10^{-7} rad^{-1} (radiation doses are expressed here in total ionizing rads in Si, although it should be noted that the fraction of proton energy that goes into production of vacancy-interstitial pairs, the nonionizing energy loss, is about 1/2000 of the total ionizing dose [17].) This degradation is significant: if the device is subjected to 1000 rad yr^{-1} and there are 1000 transfers necessary to clock out the charge, then 40% of the charge packet would be lost due to proton-induced defects. At higher illumination levels, the traps greatly complicate the device response, particularly in single-photon counting applications. In this case, for example, the spectral response of the CCD becomes a function of the spatial distribution of the incident radiation.

© 1999 by CRC Press LLC

This loss of CTE can be circumvented in several ways, including the use of increased shielding, a fat zero, annealing out the damage, implanting a narrow trough along the direction of transfer in the buried channel, or operating the device at a different (generally lower) temperature.

Relatively thick shielding, up to the equivalent 4 to 5 cm (1.6 to 2 inch) of aluminum, can provide significant attenuation (factors of several) of proton dose encountered in the radiation belts [18]. A fat zero is a uniform charge added to all the pixels of the CCD, usually induced by flooding the CCD with a low light level. Although a fat zero can reduce the CTE loss by filling the traps so they cannot be occupied by electrons from the charge packet of interest, they also add to the noise of the system. The P–V complex will dissociate at temperatures around 135° C [19], but the annealing is incomplete and may interfere with other requirements or constraints of the satellite mission. Using photolithography, a narrow trough or notch can be included in the buried channel parallel to the direction of transfer during fabrication, so charge packets are kept constrained and are less likely to interact with traps generated randomly across the buried channel [20]. It is not difficult to introduce a channel that is approximately 2 μm wide and can handle a charge packet of tens of thousands of electrons; this can decrease the CTE loss to 7×10^{-8} rad^{-1} or less. Reducing the operating temperature slows the kinetics of trap emptying [21], so a single electron can be lost from the charge packet and fill the trap for the integration time of the frame. The effectiveness of this process depends on the clock speed and integration time, as well as the ability to operate the CCD at temperatures that approach –150° C, but CTE loss can be as low as 10^{-8} rad^{-1} if troughs are included with low-temperature operation. Cosmic rays and electrons can also cause damage by displacing Si atoms from the lattice, but the flux of cosmic rays is much lower than protons in low Earth orbits and the electrons are much less effective in creating a vacancy. The approaches to hardening against proton damage will also be effective with these latter two particles.

The major effect of electrons on CCDs is to shift the flatband voltage of the CCDs and MOSFETs, but for doses around 1000 rads, this change is on the order of 10 mV. If further hardening of the gate oxide is desired, it can be accomplished using established methods [22]. The passage of electrons and other energetic charged particles through a device also creates free carriers that constitute an interfering signal. One electron-hole pair is created for each 3.65 eV absorbed in the Si, and charged particles can deposit charge packets of up to a full-well level and more, depending on the species, energy, and the active depth of the device. In astronomy, such events are an annoyance, even in terrestrial observatories, and are removed by comparing images of the same scene. In some applications, such as x-ray spectroscopy, these events are more serious because they can masquerade as desired signals unless careful analysis of the data is performed to exclude them. On the other hand, this sensitivity to charged particles can actually be used to advantage. The known conversion between particle energy deposition and liberated charge means that CCDs can be used as spectroscopic detectors, and such an application has been proposed for inertial-confinement fusion diagnostics [23].

Radiation hardening of CCDs has made rapid progress in the last few years, allowing devices to have much longer lives for scientific applications. Fabrication and operational changes have increased the hardness to displacement damage and the process requirements of high-quality ICs have led to a gate dielectric that is quite robust to ionizing radiation.

References

1. C.K. Kim, The physics of charge-coupled devices, in M.J. Howes and D.V. Morgan, (Eds.), *Charge-Coupled Devices and Systems,* Wiley, New York (1979).
2. R.P. Kraft, D.N. Burrows, G.P. Garmire, J.A. Nousek, J.R. Janesick, and P.N. Vu, Soft x-ray spectroscopy with sub-electron readnoise charge-coupled devices. *Nucl. Instr. & Meth.,* A361, 372–383, 1995.
3. D.N. Burrows, G.D. Berthiaume, M.A. Catalano, G.P. Garmire, C. Larkin, F. Marks, J.A. Nousek, and G.M. Weaver, Penn State imaging x-ray spectrometer, EUV, X-ray, and gamma-ray instrumentation for astronomy and atomic physics, eds. C.J. Hailey and O.H.W. Siegmund, *Proc. SPIE,* 1159, 92–104, 1989.

© 1999 by CRC Press LLC

4. C.E. Chandler, R.A. Bredthauer, J.R. Janesick, J.A. Westphal, and J.E. Gunn, Sub-electron noise charge coupled devices. *SPIE Symp. on Electronic Imaging, Proc. SPIE,* 1242, 238–251, 1990.
5. R.P. Kraft, D.N. Burrows, G.P. Garmire, and J.A. Nousek. Thin-gate front side-illuminated versus back side-illuminated charge-coupled devices for X-ray astronomy. *Astrophysical J. Lett.,* 466, L51–L54, 1996.
6. M.C. Weisskopf, S.L. O'Dell, R.F. Elsner, and L.P. Van Speybroeck, Advanced X-ray Astrophysics Facility (AXAF): an overview. *Proc. SPIE,* 2515, 312–329, 1995.
7. Y. Matsunaga and S. Ohsawa, Analysis of low signal level characteristics for high-sensitivity CCD charge detector. *Trans. Electron Devices*, 39, 1465–1468, 1992.
8. D.F. Edwards, *Handbook of Optical Constants of Solids,* E.P. Palik, Ed., New York: Academic Press, 1985, 547.
9. B.L. Henke, P. Lee, T.J. Tanaka, R.L. Shimabukuro, and B.K. Fujikawa, Low energy X-ray diagnostics. D.T. Attwood, B.L. Henke, Eds., *AIP Conf. Proc. No. 75,* New York: American Institute of Physics, 1981, p. 340.
10. J.R. Janesick, D. Campbell, T. Elliott, and T. Daud, Flash technology for charge-coupled-device imaging in the ultraviolet. *Opt. Eng.,* 26: 852–863, 1987.
11. B.E. Burke, J.A. Gregory, R.W. Mountain, J.C.M. Huang, M.J. Cooper, M.J., and V.S. Dolat, High-performance visible/UV CCD imagers for space-based applications. *Proc. SPIE* 1693, 86–100, 1992.
12. M.P. Lesser, Improving CCD quantum efficiency, *Inst. in Astronomy VIII, Proc. SPIE,* 2198, 782–791, 1994.
13. M.E. Hoenk, P.J. Grunthaner, F.J. Grunthaner, R.W. Terhune, M. Fattahi, and H.-F. Tseng, Growth of a delta-doped silicon layer by molecular beam epitaxy on a charge-coupled device for reflection limited ultraviolet quantum efficiency. *Appl. Phys. Letts.* 61, 1084–1086, 1992.
14. C.M. Huang, B.E. Burke, B.B. Kosicki, R.W. Mountain, P.J. Daniels, D.C. Harrison, G.A. Lincoln, N. Usiak, M. A. Kaplan, and A.R. Forte, A new process for thinned, back-illuminated CCD imager devices. *Proc. Intl. Symp. VLSI Technol., Syst., Appl.,* New York: IEEE, 1989, 98–101.
15. F. Scholze and G. Ulm, Characterization of a windowless Si(Li) detector in the photon energy range 0.1–5 keV. *Nucl. Instr. Meth.,* A339, 49–54, 1994.
16. G. Prigozhin, M. Bautz, S. Kissel, G. Ricker, S. Kraft, F. Scholze, R. Thornagel, and G. Ulm, Absolute measurement of oxygen edge structure in the quantum efficiency of X-ray CCDs, *IEEE Trans. Nucl. Sci.,* 44, 970–975, 1997.
17. M.J. Cantella, B.E. Burke, J.A. Gregory, D.C. Harrison, E.D. Savoye, and B.-Y. Tsaur, Large silicon staring-array sensors, *Infrared Focal Plane Arrays IIIA,* J. A. Jamieson (Ed.), Washington: Ballistic Missile Defense Organization, 1994, 10-1–10-76.
18. K.C. Gendreau, M.W. Bautz, and G.R. Ricker, Proton damage in X-ray CCDs for space applications: ground evaluation techniques and effects on flight performance. *Nucl. Inst. Meth.* A335, 318–327, 1993.
19. M. Hirata, H. Saito, and J. Crawford, Effect of impurities on the annealing behavior of irradiated silicon. *J. Appl. Phys.* 38, 2433–2438, 1967.
20. T.S. Villani, W.F. Kosonocky, F.S. Shallcross, J.V. Groppe, G.M. Merais, J.T. O'Neill III, and B.J. Esposito, Construction and performance of a 320×244-element IR-CCD imager with PtSi Schottky-barrier detectors. *Proc. SPIE,* 1107, 9–21, 1989.
21. K.C. Gendreau, G.Y. Prigozhin, R.K. Huang, and M.W. Bautz, A technique to measure trap characteristics in CCDs using X-rays. *IEEE Trans. Electron Dev.,* 42, 1912–1917, 1995.
22. P.V. Dressendorfer, Effects of radiation on microelectronics and techniques for hardening. In T. P. Ma and P. V. Dressendorfer (Eds.), *Ionizing Radiation Effects in MOS Devices and Circuits,* New York: John Wiley & Sons, 1989, 333.
23. B.E. Burke, R.D. Petrasso, C.-K. Li, and T.C. Hotaling, Use of charge-coupled device imagers for charge-particle spectroscopy, *Rev. Sci. Inst.,* 68: 599–602, 1997.
24. G.H. Jacoby (Ed.), *CCDs in Astronomy,* San Francisco: Astronomical Society of the Pacific, 1990.

© 1999 by CRC Press LLC